NASA-CR-192433

FINAL REPORT

for

NASA contract NAS8-36955 to the University of Alabama in Huntsville: Delivery Order No. 103

Prepared by:

J. L. Horwitz
Department of Physics/ Center for Space Plasma and Aeronomic Research
The University of Alabama in Huntsville
Huntsville, Alabama 35899
October 1992

The objective of this delivery order was to make modifications in infrared radiative transfer modeling programs and inversion techniques for remote sensing of the Earth's atmosphere and planetary atmospheres. The work on this delivery was based on the involvement of several UAH students, working primarily under the supervision of Dr. M. Abbas of MSFC. The periods worked by the students were:

Student Name	Period Worked
C.-H. Lin	10/90-12/90
C. Keffer	6/91(2 weeks)
R. Cleary	12/91-5/92
C. Noun	12/91 and 6/92
A. Joshi	2/92-5/92
K.-H. Kim	2/92-9/92
I. Sawaneh	6/92-9/92

The purpose of this work was to assist with the development of analytical techniques for the interpretation of infrared observations. We have (1)helped to develop models for continuum absorption calculations for water vapor in the far infrared spectral region; (2) worked on models for pressure-induced absorption for O_2 and N_2 and their comparison with available observations; and (3) developed preliminary studies of non-local thermal equilibrium effects in the upper stratosphere and mesosphere for infrared gases.

These new techniques were employed for analysis of balloon-borne far infrared data by Traub's group at the Harvard-Smithsonian Center for Astrophysics. The empirical continuum absorption model for water vapor in the far infrared spectral region, and the pressure-induced N_2 absporption model were found to give satisfactory results in the retrieval of the mixing rations of a number of stratospheric trace constituents from balloon-borne far infrared observations. A presentation on this work was presented at the Spring meeting of the American Geophysical Union, and a full paper

has been accepted for publication in the Journal of Geophysical Research. Copies of the presentation abstract and the accepted paper are attached.

(Atmospheres), December, 1992

Stratospheric Minor Constituent Distributions from Far-Infrared Thermal Emission Spectra

Mian M. Abbas
Space Science Laboratory
NASA Marshall Space Flight Center, Huntsville, Alabama

Wesley A. Traub
Harvard-Smithsonian Center for Astrophysics
Cambridge, Massachusetts

16 August 1992; JGRd-1255

Abstract

We retrieve mixing ratio profiles of O_3, $H_2{}^{16}O$, $H_2{}^{17}O$, $H_2{}^{18}O$, HF, and HCl from far-infrared thermal emission observations of the limb in the 80-220 cm^{-1} spectral region. The observations were made with a balloon-borne Fourier-transform spectrometer as a part of the 1983 Balloon Intercomparison Campaign (BIC-2). A subset of the data was analyzed previously using the method in *Traub et al.* [1982, 1991]; in the present paper, we use an alternative method of calibration and analysis, given in *Abbas et al.* [1985]. The retrieved constituent profiles are compared with the measurements made with other instruments on the BIC-2 flights. The results for the concentrations of $H_2{}^{17}O$ and $H_2{}^{18}O$ obtained in this study indicate no isotopic enhancement or depletion with a standard deviation of about 20%.

1. Introduction

Far-infrared thermal emission spectroscopy provides a powerful tool for studies of stratospheric thermal structure and constituent distributions, via the numerous rotational transitions in this spectral region. Stratospheric limb observations of thermal emission spectra having high spectral resolution and high sensitivity can be analyzed to retrieve vertical profiles of temperature and constituent species abundances. Some recent results from far-infrared spectra obtained with high altitude balloon-borne instruments include: H_2O, $H_2{}^{17}O$, $H_2{}^{18}O$, HDO, $^{16}O^{16}O^{18}O$, $^{16}O^{18}O^{18}O$ [*Abbas et al.*, 1984b, 1985; *Carli and Park*, 1988; *Dinelli et al.*, 1991; *Guo et al.*, 1989; *Rinsland et al.*, 1991]; CO [*Abbas et al.*, 1988]; HCN [*Abbas et al.*, 1987b, *Carli and Park*, 1988]; HF, HCl [*Carli and Park*, 1988; *Park and Carli*, 1991]; $O(^3P)$ [*Lin et al.*, 1987]; HOCl [*Chance et al.*, 1989]; HO_2, OH,

H_2O_2 [*Traub et al.*, 1990; *Chance et al.*, 1991a; *Park and Carli*, 1991]; HBr [*Park et al.*, 1989; *Traub et al.*, 1992].

After the surprising measurements indicating an enhancement in stratospheric heavy ozone concentrations [*e.g.*, *Maursberger*, 1981, 1987; *Abbas et al.*, 1987c; *Goldman et al.*, 1989], there has been a considerable amount of interest in observing the isotopic distribution of other constituents, in particular of water vapor. Theoretical considerations [*Kaye*, 1987, 1990] indicate a small depletion in the stratospheric $H_2{}^{18}O$ distribution relative to normal water vapor. Measurements by *Carli et al.* [1990] from far-infrared thermal emission observations and *Rinsland et al.* [1991] from middle infrared solar absorption observations showed no enhancements or small depletions indicating agreement with the theoretical predictions. Inconsistent with with the two latter investigations, the results obtained by *Guo et al.* [1989] showed substantial relative enhancements in the $H_2{}^{18}O$ concentration.

We report here the results of an analysis which was carried out with two objectives in mind. The first objective is to analyze the existing set of 1983 far-infrared spectra for O_3, H_2O, HF, and HCl using a method of calibration, angle determination, and analysis which was developed independently from that originally used on a subset of this data. The second objective is to analyze the spectra for $H_2{}^{17}O$ and $H_2{}^{18}O$, which has not been done previously, and to compare these results with those of other investigations.

2. Observations

Far-infrared stratospheric limb thermal emission spectra were obtained with a double-beam Fourier-transform spectrometer [*Traub et al.*, 1982, 1991] launched on a balloon flight from Palestine, Texas, on June 23, 1983, as part of the Balloon Intercomparison Campaign (BIC-2). The spectra analyzed in this paper were obtained between about 10 am and 10 pm local time at a float altitude of about 37 km. The field of view is a circular beam with 0.3deg full width at half maximum, which corresponds to a vertical resolution of about 2 km at the limb. The telescope pointing direction is controlled in azimuth to about 1deg by the gondola, and in elevation by a single-axis stabilization system which employs a gyroscope for short term reference (gondola sway) and an inclinometer for long term reference (gondola tilt).

The usable spectral range is about 80 to 220 cm^{-1}, and the unapodized spectral resolution is 0.032 cm^{-1}. A complete limb-scan sequence comprises spectral observations at seven angles: a black-body reference, a high-elevation background scan, and five scans near the limb with tangent heights from 21 to 37 km. Three segments of the observed, calibrated, summed spectra from a complete limb sequence are shown in Figs. 1-3. Selected

spectral features due to the rotational lines of O_3, $H_2{}^{16}O$, $H_2{}^{17}O$, $H_2{}^{18}O$, HF, HCl, and O_2 are identified.

3. Calibration and Angle Determination

One purpose of the present paper is to give an alternative analysis of the observations discussed above. In this section we discuss common and different features in both the calibration and the angle determination.

That part of the calibration, which is common to both methods, is as follows. Raw spectra are intensity-calibrated by subtracting a "cold" background spectrum and dividing by the difference of a "hot" reference blackbody spectrum and the cold spectrum. The cold spectrum is derived from an upward-looking atmospheric spectrum; the narrow emission lines are clipped off numerically, and the result smoothed so as to preserves all instrumental features, such as the filter bandpass and window interference fringes. The hot spectrum is derived from a spectrum of the on-board blackbody, similarly smoothed. Raw spectra of the stratosphere are converted to an absolute flux scale by subtracting a cold spectrum, dividing by the difference of the hot and cold spectra, and multiplying by the Planck function corresponding to the measured temperature of the reference blackbody. These temperatures were measured with 3 thermistors which were calibrated by the manufacturer and checked before installation by a water-ice triple point measurement; the measurement precision was smaller than 1 K. Nadir-referenced limb-viewing angles were measured by an on-board single-axis platform which was referenced to a low-drift gyro and inclinometer [*Coyle et al.*, 1986; *Traub et al.*, 1986]; the precision of pointing was about 0.02deg.

The first method (hereafter "Method 1") is as follows. (a) The onion-peel, non-linear least-squares retrieval method is the same as used to obtain all previously published profiles from the FIRS-1 and -2 instruments, as discussed in previous publications [*e.g., Traub et al.*, 1982, 1991]; (b) The intensity calibration of the data relies on the in-flight determination of the reference black-body temperature. (c) The pointing angles are controlled by the on-board pointing system [*Coyle et al.*, 1986; *Traub et al.*, 1986]. Method 1 was employed to retrieve constituent profiles from data obtained by FIRS-1 flown on BIC-2, and by FIRS-2 on subsequent balloon flights. In particular, profiles from BIC-1 have been published for H_2O [*Murcray et al.*, 1990], O_3 [*Robbins et al.*, 1990], HF [*Mankin et al.*, 1990], and HCl [*Farmer et al.*, 1990]. These 4 papers show that the FIRS-1 profiles are in very good agreement with those of the other investgators in the BIC campaign, with the exception of H_2O, for which the FIRS-1 profile is higher than average. Thus, except for the reasons cited in the following paragraph, we have, *a priori*, no reason to doubt the accuracy of Method 1.

The second method (hereafter "Method 2"), constituting the alternative analysis discussed in this paper, is as follows. (a) The onion-peel, non-linear least-squares inversion technique is the same as that discussed in previous publications [*Abbas et al.*, 1984a,b; 1985; 1987a,b,c, 1988]. (b) The flux intensity scale is calibrated using the observed fluxes at the peaks of saturated emission lines. (c) The pointing angles are obtained from an analysis of three observed O_2 lines at 83.469, 85.349, and 106.421 cm^{-1}.

The reasoning behind our Method-2 adjustment of the intensity scale is the following. In principle, the intensity of any optically thick spectral line should depend only on the atmospheric temperature profile. However, we found that the observed peak intensities of fully saturated H_2O lines, which should reflect atmospheric temperatures in the vicinity of the balloon float height, were slightly smaller than the values calculated with the radiative transfer model. In order to match the peak intensities of the observed and calculated lines, the obgserved spectra were multiplied by a factor of 1.02 to 1.03, depending on the wavenumber. This implies that the reference blackbody is actually about 3 to 4 K warmer than the thermisters indicated.

The reasons for employing the pointing angles retrieved from the observed spectra are two-fold. (*i*) The mixing ratio profile of H_2O (and to a much lesser extent O_3, HF, and HCl) retrieved by employing the nadir angles from Method 1 appeared to be systematically higher than the average of other experiments on the same gondola. (*ii*) More striking however, we found that the three observed O_2 lines were poorly matched by the calculated lines when we used the standard O_2 mixing ratio and the nadir angles from Method 1. This discrepency could arise partly from errors in the AFGL O_2 line-broadening coefficients, since these parameters are subject to considerable uncertainties [*Chance et al.*, 1991b]. The broadening coefficient of the 83.469 cm^{-1} line of O_2 at 245 K (*priv. comm. by Nolt et al., cited in Chance et al.* [1991b]) is larger than the AFGL value by about 16%. Experimental data on the other two lines employed in the present analysis are not available. However, errors of the order of the above magnitude in the broadening coefficients are not sufficient to explain the mismatch between the observed and calculated O_2 lines.

Another possibility is that the assumed altitude of the balloon is in error. We believe that this is unlikely to be a significant effect in the present case because, according to our published error analyses [*cf. Murcray et al.*, 1990; *Robbins et al.*, 1990; *Mankin et al.*, 1990; *Farmer et al.*, 1990] the uncertainty in mixing ratio at any point in the profile is only about 3-4% for H_2O, O_3, HF, or HCl; of the seven other error sources identified in these BIC-2 studies, the estimated contribution is either about the same amount (from, for example, pointing uncertainty) or substantially larger (from pressure broadening uncertainty).

Recognizing the above uncertainties, we procede nevertheless, in the spirit of a

numerical experiment. The results for the retrieved pointing angles are as follows. From the lowest to highest viewing angle, initially corresponding to nadir angles of 86.0, 86.5, 87.2, 88.1, and 91.0deg, we find the best-fit angles to all be revised in the sense of viewing lower, by amounts .14(.02), .18(.01), .26(.02), .45(.05), and .95(.20)deg, respectively. Values in parentheses are the rms scatter of the three oxygen lines used in the calculation. The average shift is 0.40deg downward. (For completeness, we note that neither the magnitude nor the systematic variation of these angular offsets can be explained by any known properties of the pointing platform.)

In *Chance et al.* [1991b] it was pointed out that the oxygen line broadening coefficients in the AFGL catalog might be represented better by values which were about 20% larger, although it was not recommended that this correction be adopted until more extensive laboratory measurements be undertaken. To see what effect such a change in the broadening parameter might have, we repeated the above calculation with broadening parameters which were 20% larger, and found the best-fit angles to again be shifted in the sense of viewing lower in altitude, but now by amounts .04(.12), .10(.03), .17(.06), .21(.12), .56(.60)deg, respectively. Here again the values in parentheses are the rms scatter of the three lines. The average shift is 0.22deg downward. Clearly the larger broadening parameters give shifts which are about half the nominally required values, which suggests that perhaps the broadening parameters are indeed too small. However, the increased broadening parameter still requires that the viewing angles be shifted by substantial (albeit smaller) amounts; also, the rms scatter is larger, indicating poorer overall agreement between the three oxygen lines. In conclusion, this exercise shows us that (*i*) the magnitude of the angle correction increases with tangent altitude, and (*ii*) part of the correction (but not all of it) might be assignable to broadening parameter error. In the remainder of this paper, we adopt the oxygen-derived angles as determined by the nominal broadening coefficients, to give nadir angles of $86.00 - 0.14 = 86.86$, etc., and use these alternative viewing angles to derive mixing ratio profiles for the SAO BIC-2 species, plus two water vapor isotopes.

4. Abundance Analyses

The radiative transfer model and the analytical techniques employed in obtaining the results presented in this paper have been discussed in several previous publications [*e.g.*, *Abbas et al.*, 1984b, 1985, 1987a]. The model is based on full layer-by-layer and line-by-line calculations including the Earth's curvature and atmospheric refraction effects. The calculated spectra are convolved with a Hamming function having a full width at half maximum of 0.064 cm^{-1}. The molecular spectral data are from the Air Force Geophysical Laboratory 1986 edition of the trace gas compilation HITRAN [*Rothman et al.*, 1987],

which was updated to accommodate recent data for HF and HCl [*K. Chance*, priv. comm. 1991]. The temperature-pressure profile used in the analysis was obtained from radiosonde measurements near the balloon path. The spectral lines employed are listed in Table 1.

In addition to the spectral line contribution of atmospheric constituents, the radiance calculations include pressure-induced N_2 absorptions with maximum at about 90 cm^{-1}, and water vapor continuum absorptions throughout the analyzed spectral region. The pressure-induced N_2-N_2 and N_2-O_2 absorptions were calculated using a model developed at Goddard Space Flight Center [*G. L. Bjoraker*, priv. comm. 1990]. An empirical model for continuum water vapor absorption in the 80-220 cm^{-1} spectral region was constructed from the currently available observations and employed in the calculations.

The iterative inversion method employed is a nonlinear least-squares fitting technique which proceeds by successively retrieving mixing ratios from the top to the lower levels at tangent heights corresponding to the observation angles. A set of frequencies around suitable spectral lines is chosen for each observation angle such that the weighting functions are narrow and sharply peaked at the tangent heights. The spectral lines employed in the analysis are isolated, and have small values of the lower state energy in order to minimize the temperature dependence of the line strength. The effect of a finite field of view on radiative transfer and inversion calculations is negligibly small and is ignored.

5. Constituent Distributions

Using the inversion technique discussed above, vertical profiles of O_3, $H_2{}^{16}O$, $H_2{}^{18}O$, $H_2{}^{17}O$, HF, and HCl have been derived. These profiles are compared with (*i*) those obtained earlier using Method-1 calibration on a subset of the present data, (*ii*) those obtained from other data sets but using a Method-2 analysis for water isotopes, and (*iii*) those obtained independently by other groups. We expect that there could be real differences between the results of the current analysis and the previously-published (Method 1) results, owing to the fact that the current data base covers the full flight (11.0 hours of observation, looking both west and north from the balloon), whereas the previous results covered only the designated intercomparison part of the flight (1.5 hours, looking west).

5.1. Ozone

The ozone profile obtained from the 17 lines in Table 1 is shown in Fig. 4, and a comparison of the observed and calculated spectra for the ozone line at 114.16 cm^{-1} is shown in Fig. 5. The average uncertainty (1 standard deviation) of points in the retrieved profile is about 16%; this is the quadrature sum of the fitting errors (4 to 10%), pointing errors (6 to 11% of column), and line parameter errors (6% of column).

For comparison we also show the results obtained from other BIC experiments carried out on the same flight [*Robbins et al.*, 1990]: Atmospheric Environment Service (AES) in situ electrochemical cell sondes experiment; National Physical Laboratory (NPL) mid-infrared atmospheric emission grating spectrometer; and Office National d'Etudes et de Recherches Aerospatial (ONERA) infrared grille absorption spectrometer. The present profile is in general agreement with these other profiles.

Comparing the profiles from this work and the original analysis (Smithsonian Astrophysical Observatory, SAO) we see that the present profile yields smaller mixing ratios at high altitudes and larger mixing ratios at low altitudes. This may be a reflection of the corresponding O_2 curves, which have qualitatively similar shifts. Quantitatively, as noted in *Robbins et al.* [1990] the original analysis of SAO data gave a curve which differed from the BIC-2 weighted mean value (derived from 7 experiments on 2 days) by about +4% offset, with an rms scatter of 12%. By coincidence, the results of the present analysis deviate by essentially identical amounts. Thus, on balance, although the present analysis clearly yields an ozone profile which is weaker at high altitude and stronger at low altitude than the original analysis, there still is no significant difference in shift or rms with respect between either of these profiles and the BIC-2 "standard" ozone profile.

5.2. Water Vapor ($H_2{}^{16}O$)

The vertical profile for $H_2{}^{16}O$ retrieved from the 11 lines in Table 1 is shown in Fig. 6. The average standard deviation is about 15%, calculated in the same way as for ozone, above. Also shown for comparison in Fig. 6 are the measurements made by other groups in the BIC 2 campaign [*Murcray et al.*, 1990]: AES, atmospheric emission measurements in ascent in the 6.3 μm region; Denver University (DU), infrared emission measurements in the 25-26 μm region; NPL, mid-infrared emission measurements in the 1339-1350 cm^{-1} region; and SAO. The measurements by AES, NPL, and SAO were made on the balloon flight on June 20, 1983, while the DU measurements were made three days earlier on June 17.

The present profile for $H_2{}^{16}O$ is lower than that of the original SAO analysis, dropping from an average of roughly 5 ppmv to 3.5 ppmv. Part of this drop is attributable to the different methods of analysis, and part is likely due to the fact that the lines used in the original analysis were highly saturated, so the results were quite sensitive to both the intensity scale factor and the broadening coefficients. The present profile clearly falls well within the range of water profiles measured by the other BIC 2 experiments in Fig. 6, instead of being well above the range as was the case from the original analysis. (But of course this does not insure that the result is correct, because the other measurements shown have considerable scatter themselves. Indeed, on a climatological basis, one might

expect to see a monotonic increase with height, from about 3.5 ppmv near 20 km to about 4.8 ppmv near 40 km, which does not match any of the curves shown in Fig. 6.)

A comparison of the observed (solid line) and synthetic (dashed line) spectra for a typical line of $H_2{}^{16}O$ is shown in Fig. 7, indicating a good fit of the peak intensities, the continuum, and the line shapes.

5.3. $H_2{}^{18}O$

The present retrieval of $H_2{}^{18}O$ is based on 10 spectral lines identified in Table 1. The derived profile, with the mixing ratios normalized to their natural abundances in accordance with the HITRAN data base, is shown in Fig. 8. The error bars represent the total standard deviation of the measurement, calculated as the quadrature sum of the random and systematic errors. Also shown on the same figure is the simultaneously measured $H_2{}^{16}O$ mixing ratio profile (circles) discussed just above. The next figure shows a comparison of the observed (solid line) and the synthetic spectra (dashed line) indicating a good fit of some lines employed in the analysis.

In Fig. 8 we see that the $H_2{}^{18}O$ and $H_2{}^{16}O$ profiles are almost identical. No enhancement or depletion of the heavier isotope is seen. The ratio of the two profiles is essentially unity, with an average standard deviation of the ratio of about 20%. This result is in good agreement with two previous findings: *Rinsland et al.* [1991], from an analysis of the ATMOS Spacelab 3 infrared solar absorption spectra in the 1414 to 1690 cm^{-1} region; and *Carli et al.* [1991], from balloon-borne far-infrared observations in the 46 to 72 cm^{-1} made on a flight on October 5, 1982, during BIC 1. Both of the above referenced studies reported small depletions or no enhancements in the stratospheric $H_2{}^{18}O$ profile relative to the simultaneously measured $H_2{}^{16}O$ profile. The result of no enhancement or a small depletion in stratospheric heavy isotopic water vapor is consistent with theoretical considerations [*Kaye*, 1990].

The enigmatic results presented by *Guo, Abbas, and Nolt* [1989] indicating significant enhancements in the $H_2{}^{18}O$ concentrations are therefore inconsistent with three studies: *Carli et al.* [1991] from the same data set; *Rinsland et al.* [1991] from a different data set; and the present study.

The reason for the discrepancy in the result obtained by *Guo et al.* [1989] is not clear. It may be noted that the water vapor mixing ratios obtained by *Rinsland et al.* [1991] are generally higher by about 35-40% than those obtained by *Carli et al.* [1991] from a different data set. The $H_2{}^{16}O$ profile obtained by *Guo et al.* [1989] is almost identical to the profile obtained independently by *Carli et al.* [1991] from the same data set with a different retrieval method (see Fig. 3 of *Carli et al.*). Also, the $H_2{}^{18}O$ absolute mixing

ratio profiles of *Guo et al.* [1989] and of *Rinsland et al.* [1991] generally overlap within the error bars. The $H_2{}^{16}O$ profile of the latter reference, however, is 35-40% higher over most of the altitude range.

5.4. $H_2{}^{17}O$

The isotope $H_2{}^{17}O$ was retrieved using the 7 lines listed in Table 1. The vertical profile is shown in Fig. 10, along with that of the normal isotope. The error bars represent the total standard deviation from random and estimated systematic error. The next figure shows a comparison of observed (solid line) and synthetic spectra (dashed line) calculated with the retrieved mixing ratio profile, indicating a good fit between the two spectra.

A comparison of the mixing ratio profiles of $H_2{}^{16}O$ and $H_2{}^{17}O$ indicates that the concentrations of these two isotopes are essentially the same, within the uncertainties. As in the previous case, the ratio of the two profiles is close to unity, with an average standard deviation of the ratio of about 20%.

This result is consistent with those of *Rinsland et al.* [1991] obtained from ATMOS observations, and of *Carli et al.* [1991] obtained from BIC-2 observations, both of which reported small depletions or no significant deviation from the normal distribution within the error bars.

5.5. Hydrogen Fluoride and Hydrogen Chloride

The HF profile in Fig. 12 is derived from the two isolated lines given in Table 1. The average standard deviation is about 16%. A comparison of the observed and synthetic HF spectral line at 204.54 cm^{-1} is shown in the next figure.

In Fig. 13 the other HF profiles are as follows: SAO, as previously published, from BIC-2; Instituto di Ricerca sulla Onde Electromagnetiche (IROE), from thermal emission measurements with a balloon-borne far infrared spectrometer on October 5, 1982, during BIC 1; University of Liege (UL), from middle infrared absorption measurements with a grating spectrometer in the 4040 cm^{-1} region, from observations made on June 17, 1983; and the model prediction of *Ko and Sze* [WMO, 1985]. In contrast with case for ozone, the HF results here are not systematically shifted with respect to the SAO values, but instead there appears to be more scatter on both the high and low sides. The reason for this is not clear, but may be in part due to the steepness of the HF profile, which makes the lower layers relatively minor contributors compared to those above, making the retrieval more sensitive to noise.

The HCl profile retrieved from four spectral lines in Table 1 is shown in Fig. 14. Plots

of the observed and calculated spectra for one line are shown in the next figure. Also shown on Fig. 14 are: the average of the 5 profiles obtained by the BIC-2 experiments carried out by University of Liege, ONERA, AES, SAO, and IROE; and the model profile calculated by *Ko and Sze* [WMO, 1985, Vol. II]. As originally analysed with Method 1, the SAO mixing ratios for HCl tended to fall about 15% above the mean curve drawn through the HCl profiles measured by 5 independent instruments in BIC-2 [*Farmer et al.*, 1990]. However in the present analysis, using Method 2, the 3 upper data points fall clearly below the average curve, echoing the general pattern observed for the other species discussed in this paper.

6. Conclusions

In this paper we presented the results of an analysis which was carried out with two objectives in mind. The first objective was to analyze an existing set of 1983 far-infrared spectra for O_3, H_2O, HF, and HCl using a method of calibration, angle determination, and analysis which was developed independently from that originally used on a subset of this data. The second objective was to analyze the spectra for $H_2{}^{17}O$ and $H_2{}^{18}O$, which had not been done previously, and to compare these results with those of other investigations.

We find the following results. The current analysis (Method 2) gives mixing ratio profiles of O_3, H_2O, HF, and HCl which are often shifted significantly with respect to the original analysis (Method 1). The shifts are usually in the direction of a mean value, as determined from the other experiments which flew simultaneously, but in a few cases the shifts either overcompensate or seem to add noise. Overall, the Method-2 calibration seems to generally improve the derived profiles, but the improvement is not universal, and there is no explanation for why the on-board temperature and angle parameters should be in error by the implied amounts.

On the other hand, the determination of isotope ratios of water should be relatively independent of the above caveats, since some of the systematic effects of scaling drop out when ratios of abundances are taken. We find that there is no evidence for either enhancement or depletion of stratospheric water isotopes $H_2{}^{18}O$ and $H_2{}^{17}O$ with respect to the main isotope, with a standard deviation of about 20%.

Acknowledgements.

We thank K. V. Chance, D. G. Johnson, and K. W. Jucks for helpful comments. This work was supported in part by NASA grant NSG 5175.

References

Abbas, M. M., G. L. Shapiro, B. J. Conrath, V. G. Kunde, W. C. Maguire, A method for correction of errors in observation angles for limb thermal emission measurements, *Appl. Opt., 23,* 1862-1866, 1984a.

Abbas, M. M., J. Guo, I. G. Nolt, and B. Carli, Far-infrared remote sounding of stratospheric temperature and trace gas distributions, *J. Atmos. Chem., 2,* 145-162, 1984b.

Abbas, M. M., G. L. Shapiro, B. J. Conrath, V. G. Kunde, and W. C. Maguire, Thermal emission spectroscopy of the stratosphere from balloon platforms, in Advances in Remote Sensing Retrieval Methods, pp. 133-148, A. Deepak Publishing, Hampton, Va., 1985.

Abbas, M. M., J. Guo, B. Carli, F. Mencaraglia, A. Bonetti, M. Carlotti, and I. G. Nolt, Stratospheric O_3, H_2O, and HDO distributions from balloon-based far-infrared observations, *J. Geophys. Res., 92,* 8354-8364, 1987a.

Abbas, M. M., J. Guo, B. Carli, F. Mencaraglia, M. Carlotti, and I. G. Nolt, Stratospheric distribution of HCN from far-infrared observations, *Geophys. Res. Lett., 14,* 531-534, 1987b.

Abbas, M. M., J. Guo, B. Carli, F. Mencaraglia, M. Carlotti, and I. G. Nolt, Heavy ozone distribution in the stratosphere from far-infrared observations, *J. Geophys. Res., 92,* 13,231-13,239, 1987c.

Abbas, M. M., M. J. Glenn, I. G. Nolt, B. Carli, F. Mencaraglia, and M. Carlotti, Far-infrared measurement of stratospheric carbon monoxide, *Geophys. Res. Lett., 15,* 140-143, 1988.

Carli, B., and J. Park, Simultaneous measurement of minor stratospheric constituents with emission far-infrared spectroscopy, *J. Geophys. Res., 93,* 3851-3865, 1988.

Chance, K. V., D. G. Johnson, and W. A. Traub, Measurement of stratospheric HOCl: concentration profiles, including diurnal variation, *J. Geophys. Res., 94,* 11059-11069, 1989.

Chance, K. V., D. G. Johnson, W. A. Traub, and K. W. Jucks, Measurement of the stratospheric hydrogen peroxide concentration profile using far-infrared thermal emission spectroscopy, *Geophys. Res. Lett., 18,* 1003-1006, 1991a.

Chance, K. V., W. A. Traub, K. W. Jucks, and D. G. Johnson, On the use of O_2 spin-rotation lines for elevation angle calibration of atmospheric thermal emission spectra, *International Journal of Infrared and Millimeter Waves, 12,* 581-588, 1991b.

Coyle, L. M., G. Aurilio, J. Bortz, K. V. Chance, B. G. Nagy, G. U. Nystrom, and W. A. Traub, Design for a single-axis platform for balloon-borne remote sensing, *Rev. of Sci. Inst., 57,* 2512-2518, 1986.

Dinelli, B. M., B. Carli, and M. Carlotti, Measurement of stratospheric distributions of $H_2{}^{16}O$, $H_2{}^{18}O$, $H_2{}^{17}O$, and $HD^{16}O$ from far-infrared spectra, *J. Geophys. Res., 96,* 7509-

7514, 1991.

Farmer, C. B., *et al.*, Balloon Intercomparison Campaigns: results of remote sensing measurements of HCl, *J. of Atmos. Chem., 10,* 237-272, 1990.

Goldman, A., F. J. Murcray, D. G. Murcray, J. J. Kosters, C. P. Rinsland, J.-M. Flaud, C. Camy-peyret, and A. Barbe, Isotopic abundances of stratospheric ozone from balloon-borne high-resolution infrared solar spectra, *J. of Geophys. Res., 94,* 8467-8473, 1989.

Guo, J., M. M. Abbas, and I. G. Nolt, Stratospheric $H_2{}^{18}O$ distribution from far-infrared observations, *Geophys. Res. Lett., 16,* 1277-1280, 1989.

Kaye, J. A., Mechanism of observation of isotope fractionation of molecular species in planetary atmospheres, *Rev. Geophys., 25,* 1608-1658, 1987.

Kaye, J. A., Analysis of the origins and implications ofthe ^{18}O content of stratospheric water vapor, *J. Atmos. Chem., 10,* 39-57, 1990.

Lin, F. J., K. V. Chance, and W. A. Traub, Atomic oxygen in the lower thermosphere, *J. Geophys. Res., 92,* 4325-4336, 1989.

Mankin, W. G., *et al.*, Intercomparison of measurements of stratospheric hydrogen fluoride, *J. of Atmos. Chem., 10,* 219-236, 1990.

Maursberger, K., Measurement of heavy ozone in the stratosphere, *Geophys. Res. Lett., 8,* 935-937, 1981.

Maursberger, K., Ozone isotope measurement in the stratosphere, *Geophys. Res. Lett., 14,* 80-83, 1987.

Murcray, D. G., *et al.*, Intercomparison of stratospheric water vapor profiles obtained during the Balloon Intercomparison Campaign, *J. of Atmos. Chem., 10,* 159-179, 1990.

Park, J. H., and B. Carli, Spectroscopic measurement of HO_2, H_2O_2, and OH in the stratosphere, *J. Geophys. Res., 96,* 22,535-22,541, 1991.

Park, J. H., B. Carli, and A. Barbis, Stratospheric HBr mixing ratio obtained from far-infrared emission spectra, *Geophys. Res. Lett., 16,* 787-790, 1989.

Rinsland, C. P., M. R. Gunson, J. C. Foster, R. A. Roth, C. B. Farmer, and R. Zander, Stratospheric profiles of the ATMOS Spacelab 3 infrared solar spectra, *J. Geophys. Res., 96,* 1057-1068, 1991.

Robbins, D., *et al.*, Ozone measurements during the Balloon Intercomparison Campaign, *J. of Atmos. Chem., 10,* 181-218, 1990.

Rothman, L. S., R. R. Gamache, A. Goldman, L. R. Brown, R. A. Toth, H. M. Pickett, R. L. Poynter, J. M. Flaud, C. Camy-Peyret, A. Barbe, N. Husson, C. P. Rinsland, and M. A. H. Smith, The HITRAN database: 1986 edition, *Appl. Opt., 26,* 4058-4097, 1987.

Traub, W. A., K. V. Chance, J. C. Brasunas, J. M. Vrtilek, and N. P. Carleton, Use of a Fourier transform spectrometer on balloon-borne telescope and at the Multiple Mirror Telescope (MMT), *Proc. Soc. Photo Opt. Eng., 331,* 208-218, 1982.

Traub, W. A., K. V. Chance, D. G. Johnson, and K. W. Jucks, Stratospheric spectroscopy with the far-infrared spectrometer (FIRS-2): overview and recent results, *Proc. Soc.*

Photo Opt. Eng., 1491, 298-307, 1991.

Traub, W. A., L. M. Coyle, and K. V. Chance, Performance of a single-axis platform for balloon-borne remote sensing, *Rev. of Sci. Inst., 57,* 2519-2522, 1986.

Traub, W. A., D. G. Johnson, and K. V. Chance, Stratospheric hydroperoxyl measurements, *Science, 247,* 446-449, 1990.

Traub, W. A., D. G. Johnson, K. W. Jucks, and K. V. Chance, Upper limit for stratospheric HBr using far-infrared thermal emission spectroscopy, *Geophys. Res. Lett.,* August 1992.

World Meteorological Organization, Atmospheric Ozone, Report 16, World Met. Org., Geneva, 1985.

List of Figures

Fig. 1. A limb sequence of the observed (solid line) thermal emission spectra in the 90-95 cm^{-1} region with tangent heights varying from 21 to 37 km, plotted along with the calculated spectra (dashed line) using retrieved constituent profiles. Some of the O_3 lines employed in the analysis for retrieval of the mixing ratios are identified.

Fig. 2. A limb sequence of the observed (solid line) thermal emission spectra in the 105-110 cm^{-1} region with tangent heights from 21 to 37 km, along with the calculated spectra (dashed line) using retrieved mixing ratio profiles. Some isolated lines of $H_2{}^{16}O$, $H_2{}^{18}O$, O_3 and O_2 are identified.

Fig. 3. A limb sequence of the observed spectra (solid line) in the 197-202 cm^{-1} region with tangent heights from 21 to 37 km, plotted along with the calculated spectra (dashed line) using retrieved mixing ratio profiles. A group of three $H_2{}^{17}O$ spectral lines employed in the analysis is identified.

Fig. 4. The O_3 profile retrieved from the BIC-2 far-infrared data analyzed in this work. Also shown for comparison are the results obtained by other BIC-2 experiments on the June 20, 1983 balloon fight: NPL, ONERA, AES, and SAO with the original (Method 1) analysis.

Fig. 5. Comparison of the observed and synthetic O_3 line at 114.16 cm^{-1} for a limb sequence of five angles with tangent heights at 21, 24, 28, 32, and 37 km with increasing radiance for lower altitudes.

Fig. 6. The H_2O profile retrieved from the BIC-2 far-infrared data analyzed in this work. Also shown for comparison are the results obtained by other BIC-2 experiments on the June 20, 1983 balloon fight: AES, NPL, and SAO with an alternative analysis. The DU measurements were made on June 17, 1983.

Fig. 7. Comparison of an observed and synthetic (dashed curve) H_2O line at 155.74 cm^{-1} analyzed in this work for a limb sequence of five angles with tangent heights at 21, 24, 28, 32, and 37 km with increasing radiance for lower altitudes.

Fig. 8. The $H_2{}^{18}O$ mixing ratio profile retrieved from the BIC-2 far-infrared data analyzed in this work, normalized by the standard isotope ratio as given by the HITRAN data base. Also shown for comparison is the normal $H_2{}^{16}O$ profile retrieved in this work (from Fig. 6).

Fig. 9. Comparison of an observed and synthetic (dashed curve) $H_2{}^{18}O$ line at 207.10 cm^{-1} analyzed in this work for a limb sequence of five angles with tangent heights at 21,

24, 28, 32, and 37 km with increasing radiance for lower altitudes.

Fig. 10. The $H_2{}^{17}O$ mixing ratio profile retrieved from the BIC-2 far-infrared data analyzed in this work, normalized by the standard isotope ratio as given by the HITRAN data base. Also shown for comparison is the normal $H_2{}^{16}O$ profile retrieved in this work (from Fig. 6).

Fig. 11. Comparison of three observed and synthetic (dashed curve) $H_2{}^{17}O$ lines at 201.28, 201.44, and 201.74 cm^{-1}, analyzed in this work for a limb sequence of five angles with tangent heights at 21, 24, 28, 32, and 37 km with increasing radiance for lower altitudes.

Fig. 12. The HF profile retrieved from the BIC-2 far-infrared data analyzed in this work. Also shown for comparison are the results obtained by other BIC-2 experiments on the June 20, 1983 balloon fight: SAO, with the original analysis (Method 1), IROE from data obtained on October 5, 1982, and UL.

Fig. 13. Comparison of the observed and synthetic (dashed curve) HF line at 204.54 cm^{-1} for a limb sequence of five angles with tangent heights at 21, 24, 28, 32, and 37 km with increasing radiance for lower altitudes.

Fig. 14. The HCl profile retrieved from the BIC-2 far infrared data analyzed in this work. Also shown for comparison is the average profile compiled from the results obtained by other BIC-2 experiments UL, ONERA, AES, SAO, and IROE.

Fig. 15. Comparison of the observed and synthetic (dashed curve) HCl line at 186.390 cm^{-1} for a limb sequence of five angles with tangent heights at 21, 24, 28, 32, and 37 km with increasing radiance for lower altitudes.

Table 1. Center Frequencies (cm^{-1}) of the Analyzed Spectral Lines

O_3	$H_2{}^{16}O$	$H_2{}^{18}O$	$H_2{}^{17}O$	HCl	HF
84.1759	122.8439	91.4520	152.7300	124.8269	163.9362
84.2687	130.8519	98.0350	176.6940	145.2225	204.5404
84.8324	152.4981	121.2990	180.7670	145.4399	
90.2037	155.7379	125.7380	201.2790	186.3896	
90.6415	158.9109	147.3110	201.4410		
90.8682	160.1753	165.4180	201.6750		
91.0349	178.6202	168.4930	207.7350		
97.7587	198.0182	172.8910			
102.7913	210.8833	200.3660			
106.6300	212.6339	207.1080			
109.3157	214.8745				
112.6753					
112.7948					
113.5147					
113.6321					
114.1614					
115.3057					

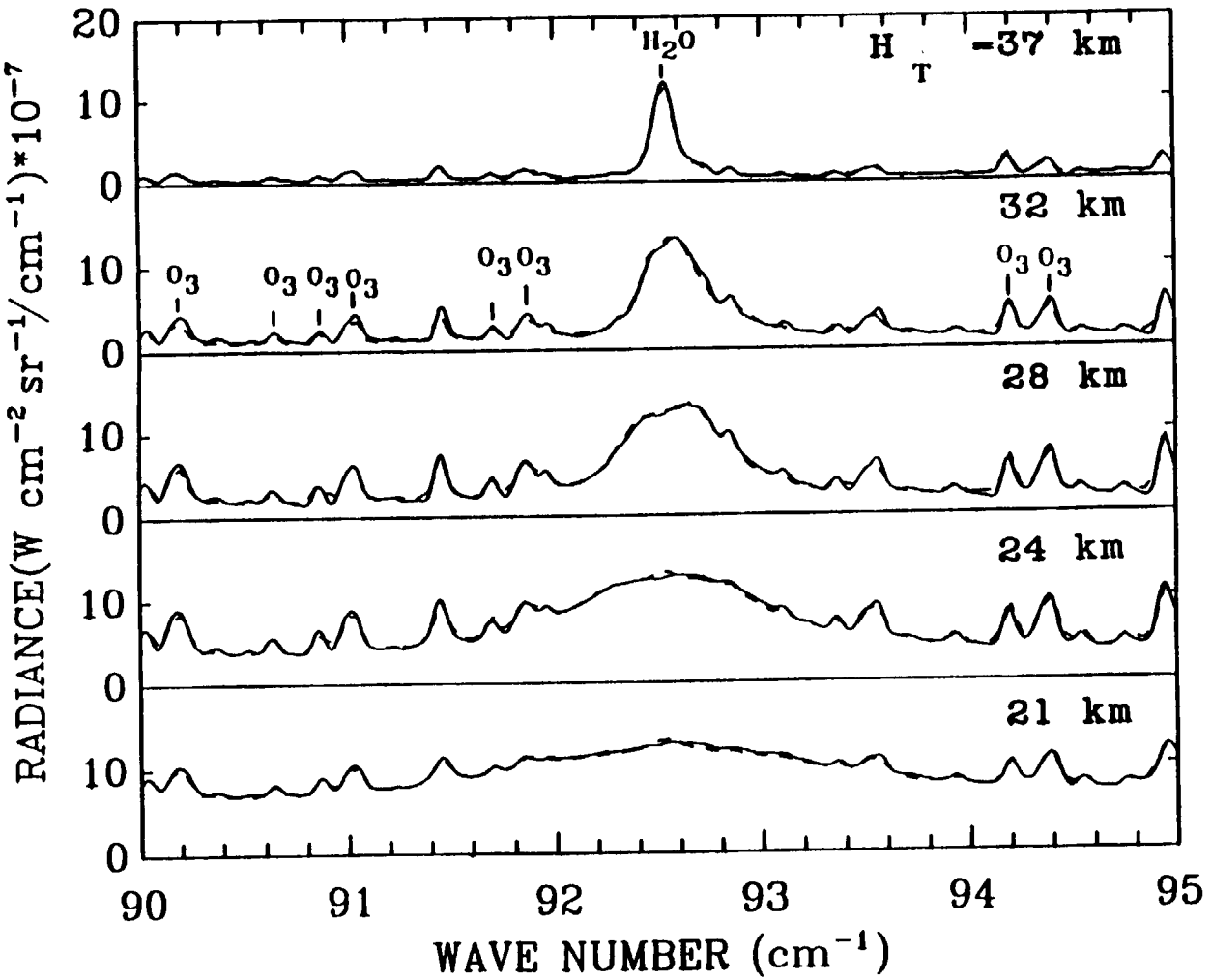
RADIANCE(W cm^{-2} sr^{-1}/cm^{-1})*10^{-7}
20
10
0
H_2O
H_T =37 km
32 km
O_3
O_3 O_3 O_3
O_3 O_3
O_3 O_3
28 km
24 km
21 km
90
91
92
93
94
95
WAVE NUMBER (cm^{-1})

Fig. 1

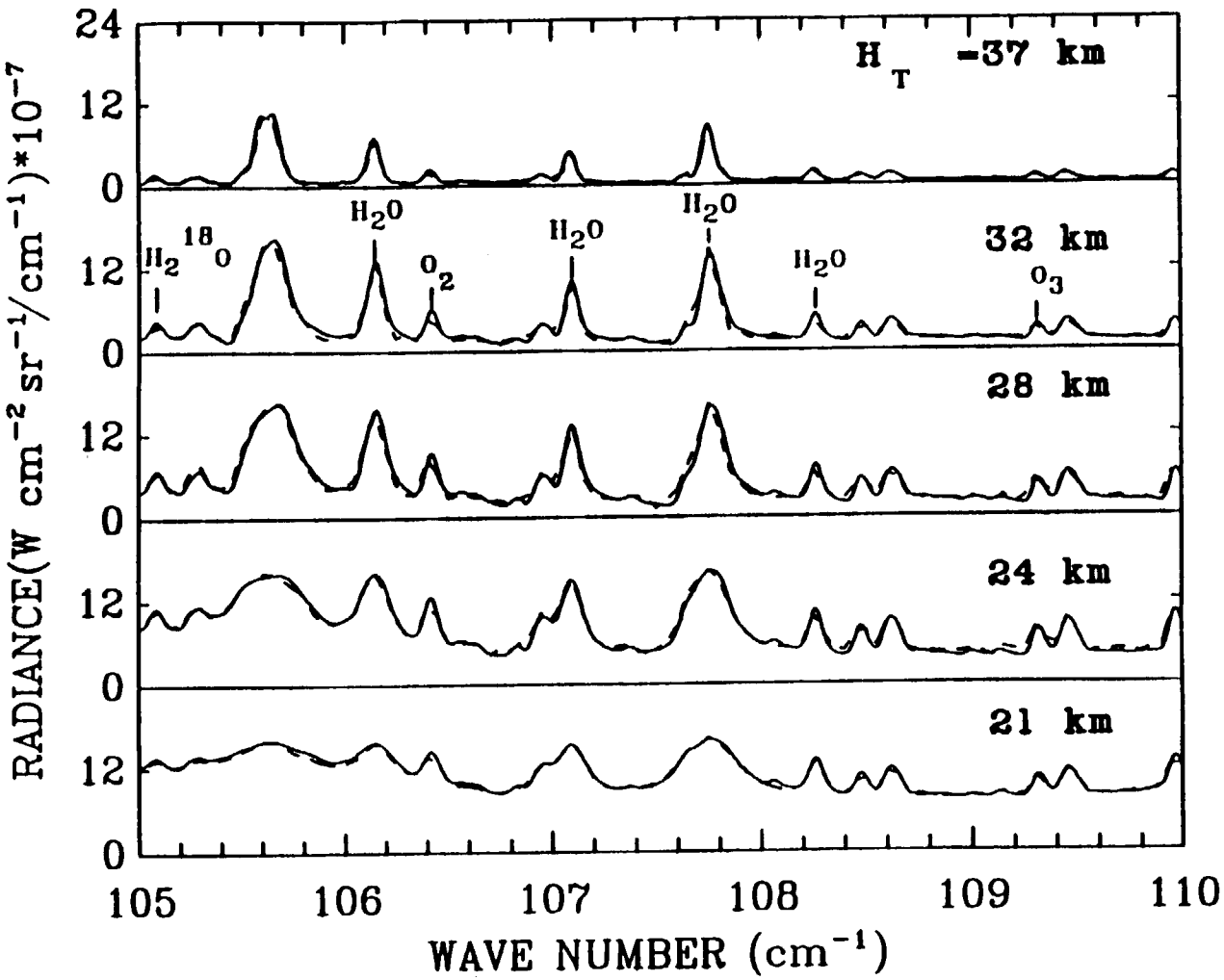
RADIANCE(W cm^{-2} sr^{-1}/cm^{-1})*10^{-7}
24
12
0
H_T =37 km
32 km
28 km
24 km
21 km
$H_2{}^{18}O$
H_2O
O_2
H_2O
H_2O
H_2O
O_3
105
106
107
108
109
110
WAVE NUMBER (cm^{-1})

Fig. 2

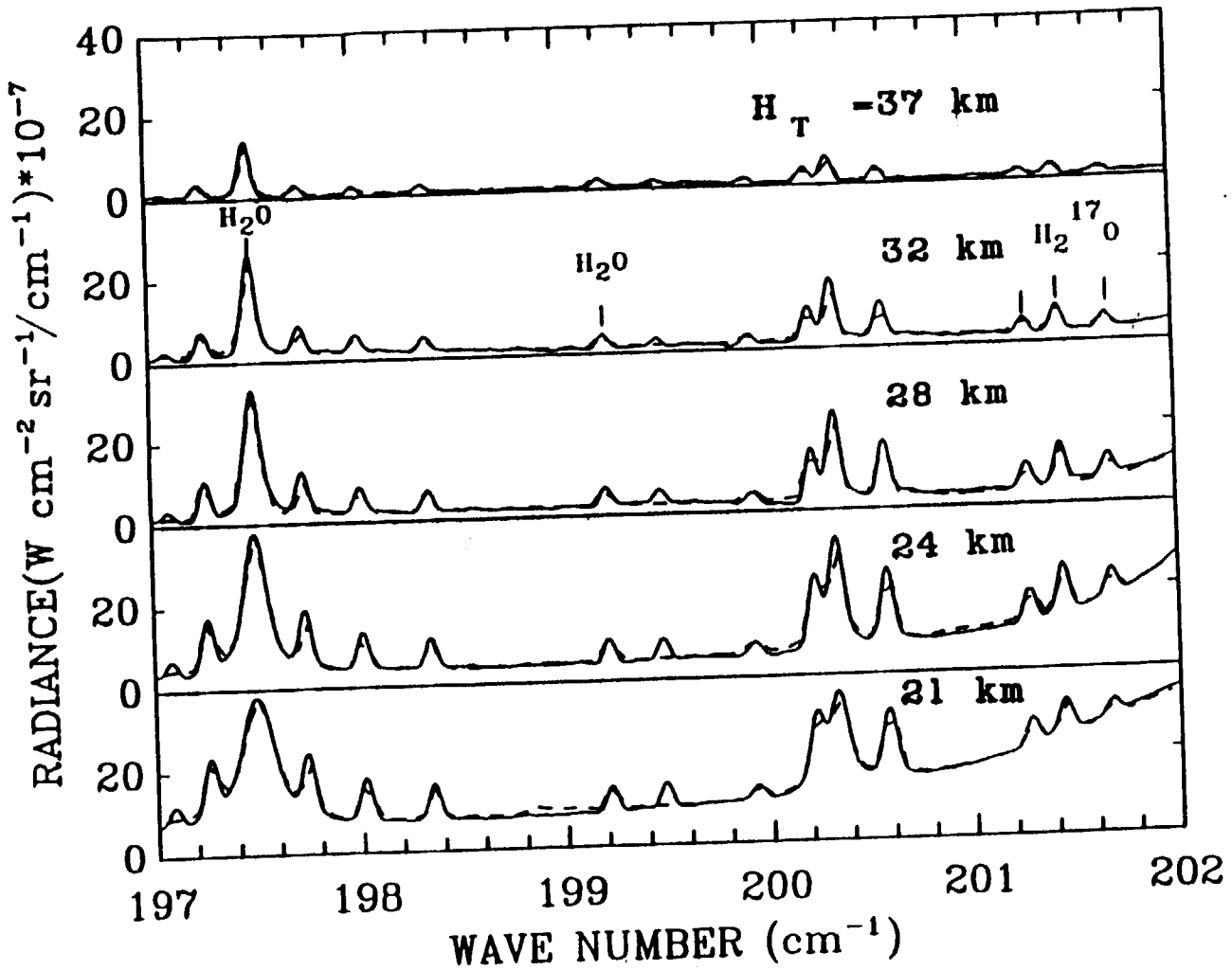
RADIANCE(W cm^{-2} sr^{-1}/cm^{-1})*10^{-7}
40
20
0
H_T =37 km
H_2O
32 km
H_2O
$H_2{}^{17}O$
28 km
24 km
21 km
197
198
199
200
201
202
WAVE NUMBER (cm^{-1})

Fig. 3

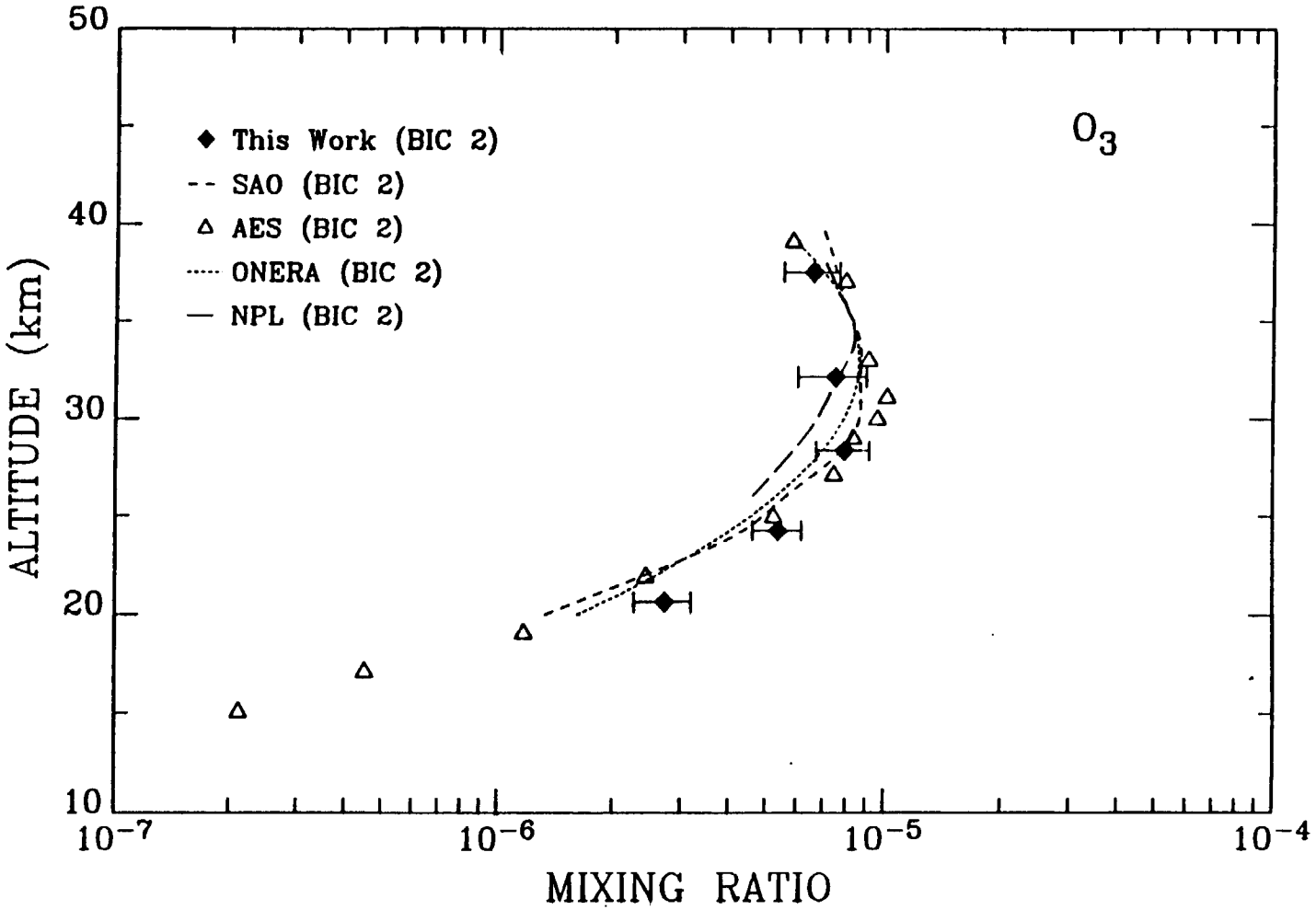
50
40
30
20
10
ALTITUDE (km)
◆ This Work (BIC 2)
-- SAO (BIC 2)
△ AES (BIC 2)
····· ONERA (BIC 2)
— NPL (BIC 2)
O_3
10^{-7}
10^{-6}
10^{-5}
10^{-4}
MIXING RATIO

Fig. 4

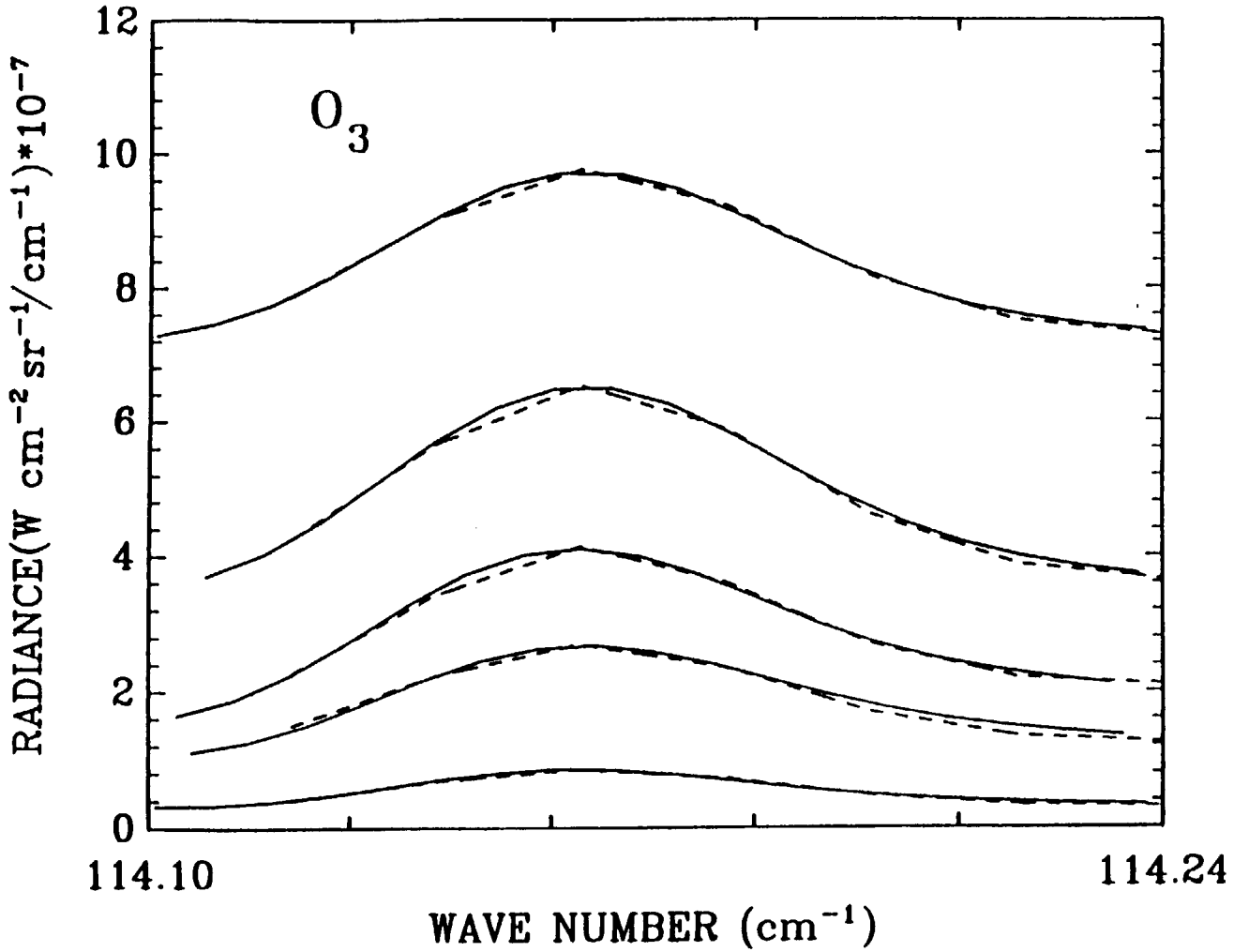
12
10
8
6
4
2
0
O_3
RADIANCE(W cm^{-2} sr^{-1}/cm^{-1})*10^{-7}
114.10
114.24
WAVE NUMBER (cm^{-1})

Fig. 5

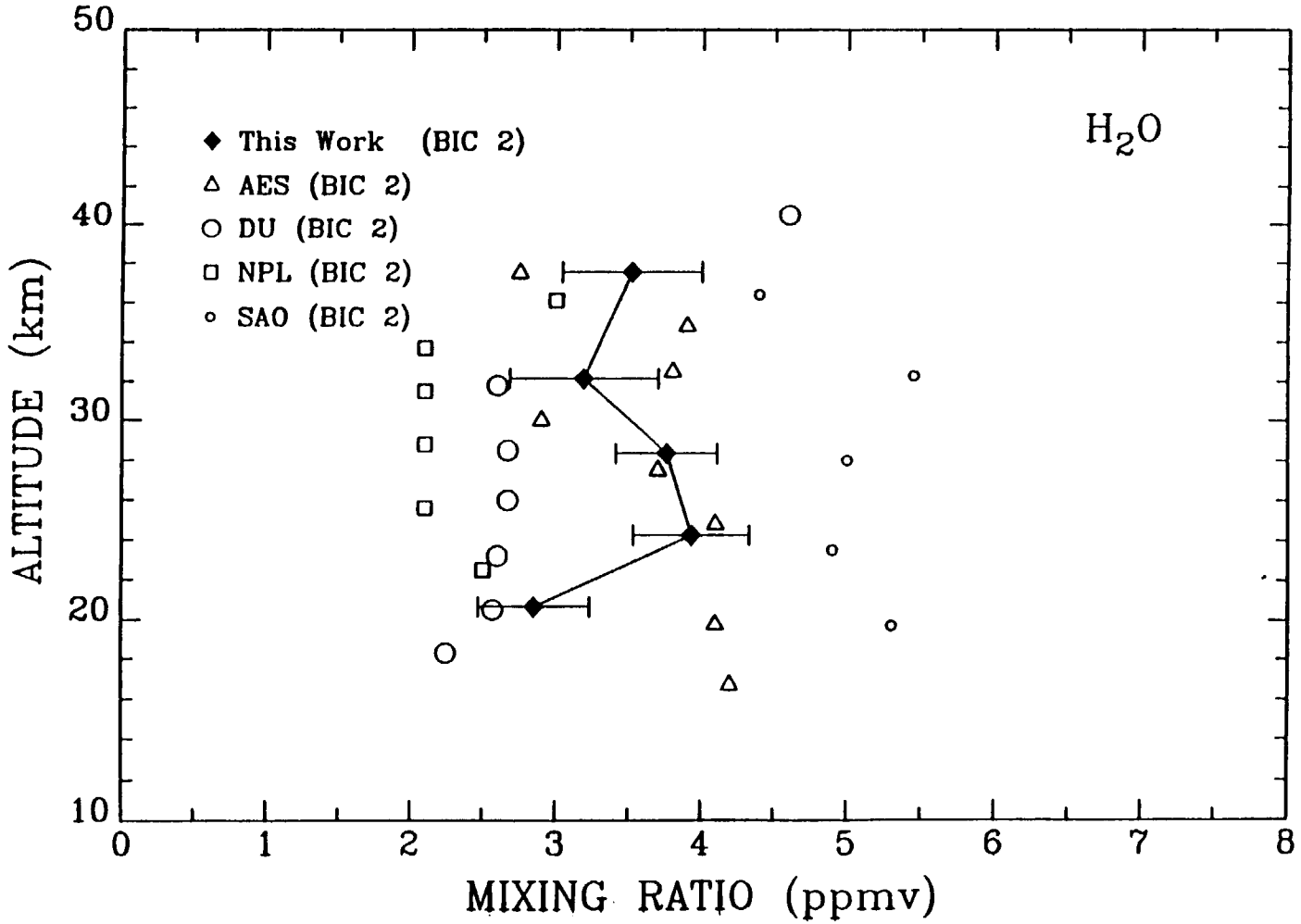
50
40
30
20
10
0
1
2
3
4
5
6
7
8
ALTITUDE (km)
MIXING RATIO (ppmv)
This Work (BIC 2)
AES (BIC 2)
DU (BIC 2)
NPL (BIC 2)
SAO (BIC 2)
H_2O

Fig. 6

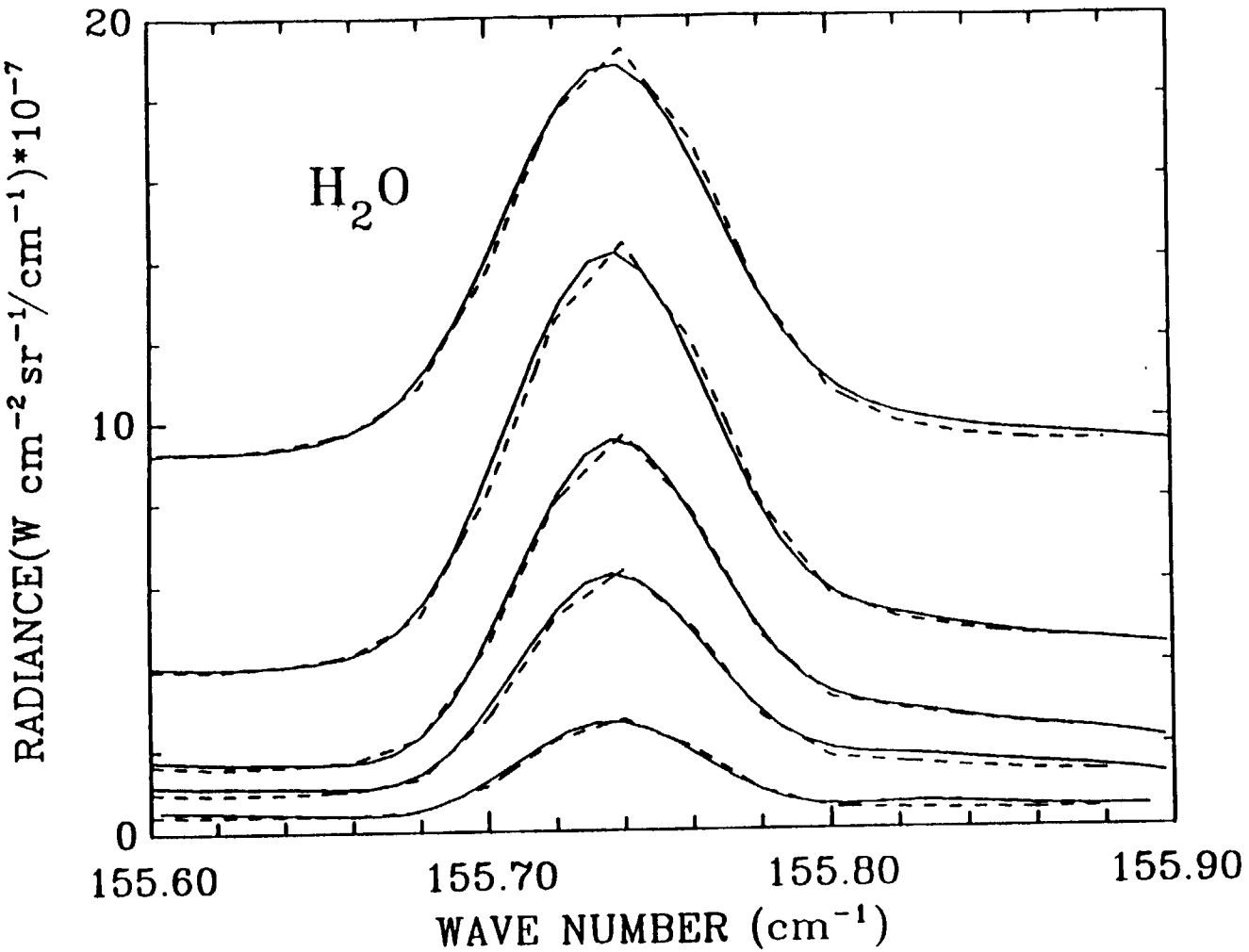
20
10
0
H_2O
RADIANCE(W cm^{-2} sr^{-1}/cm^{-1})*10^{-7}
155.60
155.70
155.80
155.90
WAVE NUMBER (cm^{-1})

Fig. 7

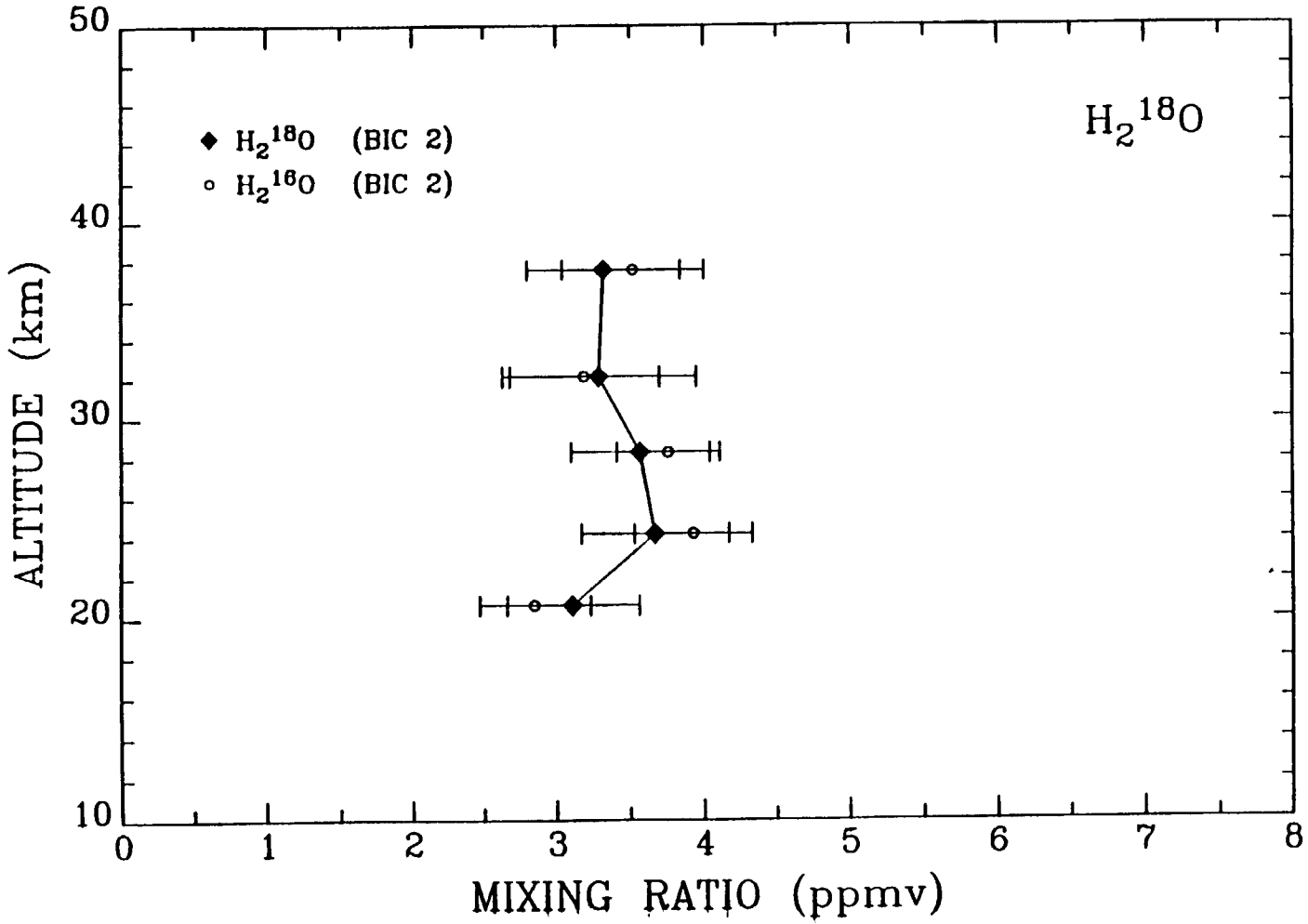
50
40
30
20
10
ALTITUDE (km)
◆ $H_2{}^{18}O$ (BIC 2)
○ $H_2{}^{16}O$ (BIC 2)
$H_2{}^{18}O$
0
1
2
3
4
5
6
7
8
MIXING RATIO (ppmv)

Fig. 8

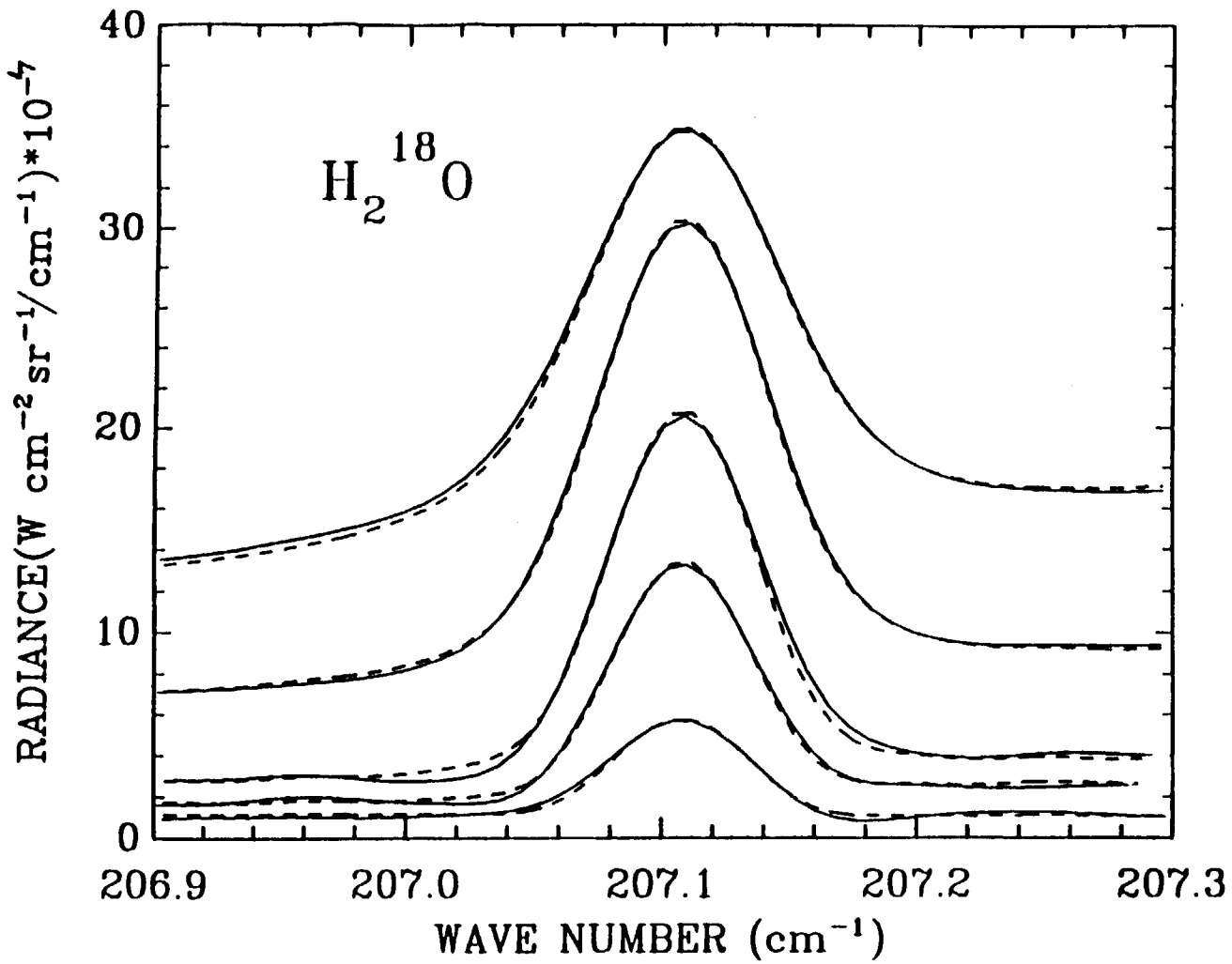
40
30
20
10
0
$H_2{}^{18}O$
RADIANCE(W cm^{-2} sr^{-1}/cm^{-1})*10^{-4}
206.9
207.0
207.1
207.2
207.3
WAVE NUMBER (cm^{-1})

Fig. 8

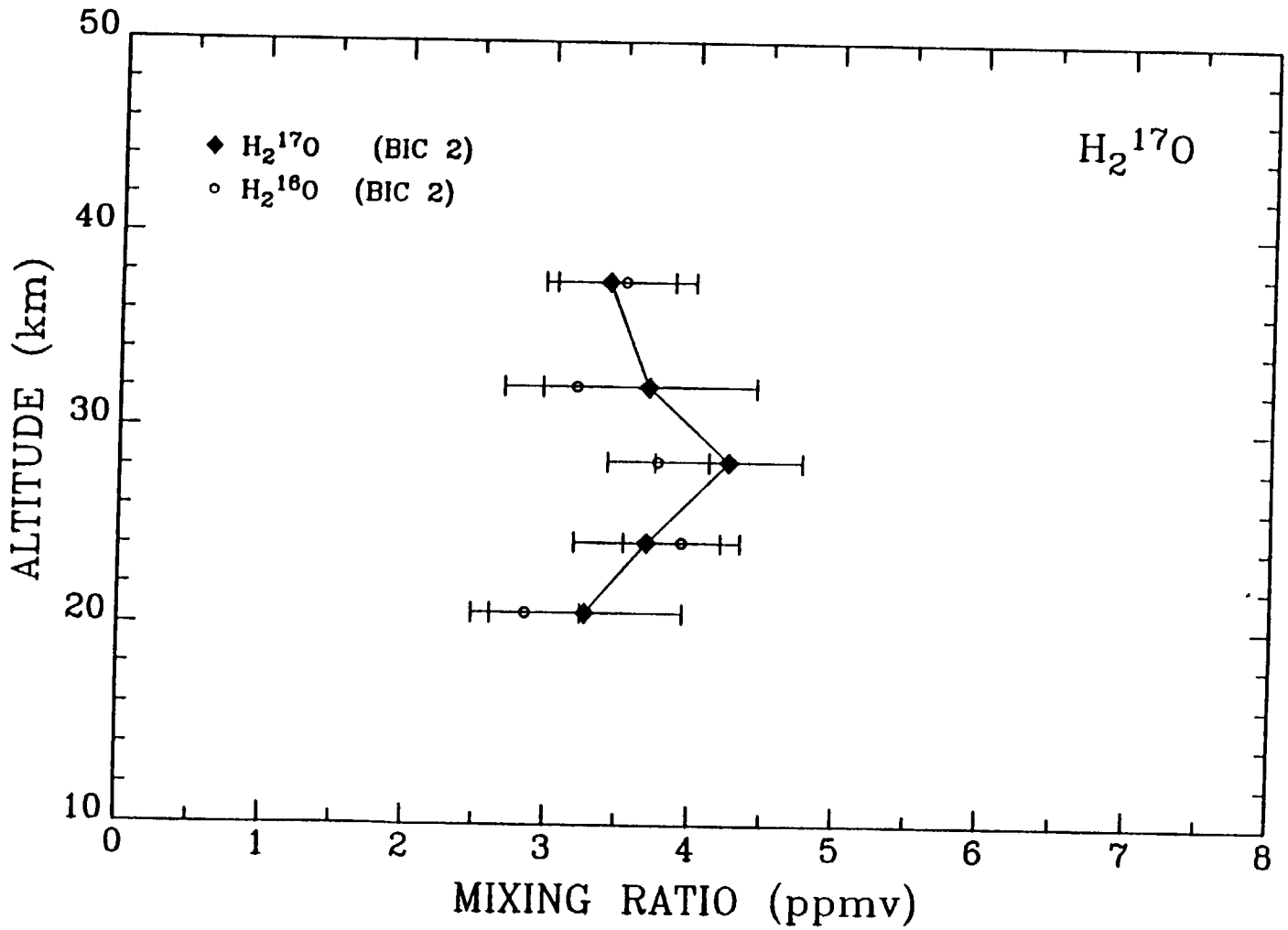
◆ $H_2{}^{17}O$ (BIC 2)
○ $H_2{}^{16}O$ (BIC 2)
$H_2{}^{17}O$
ALTITUDE (km)
50
40
30
20
10
0
1
2
3
4
5
6
7
8
MIXING RATIO (ppmv)

Fig. 9/10

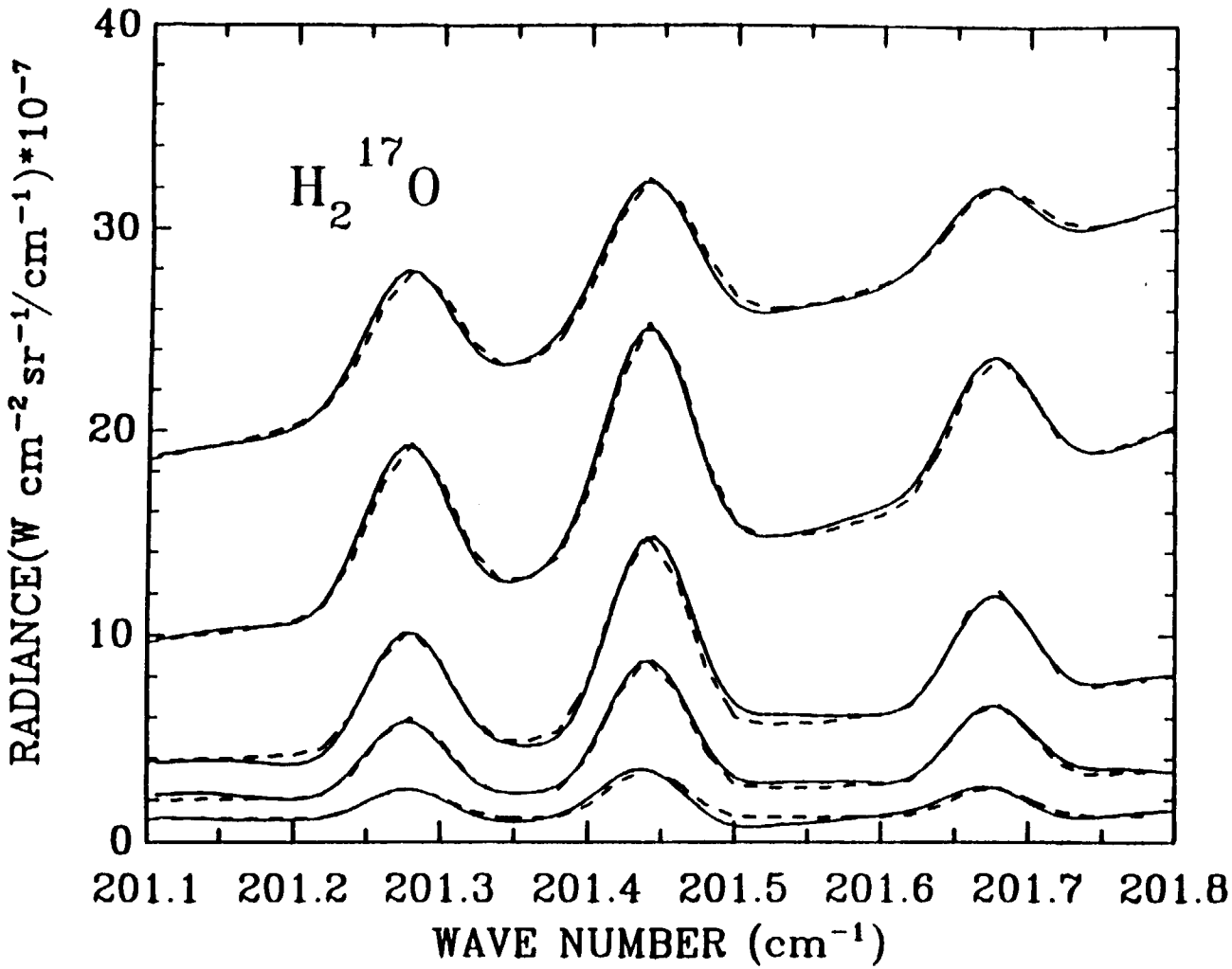
40
30
20
10
0
$H_2{}^{17}O$
RADIANCE(W cm^{-2} sr^{-1}/cm^{-1})*10^{-7}
201.1 201.2 201.3 201.4 201.5 201.6 201.7 201.8
WAVE NUMBER (cm^{-1})

Fig. 11

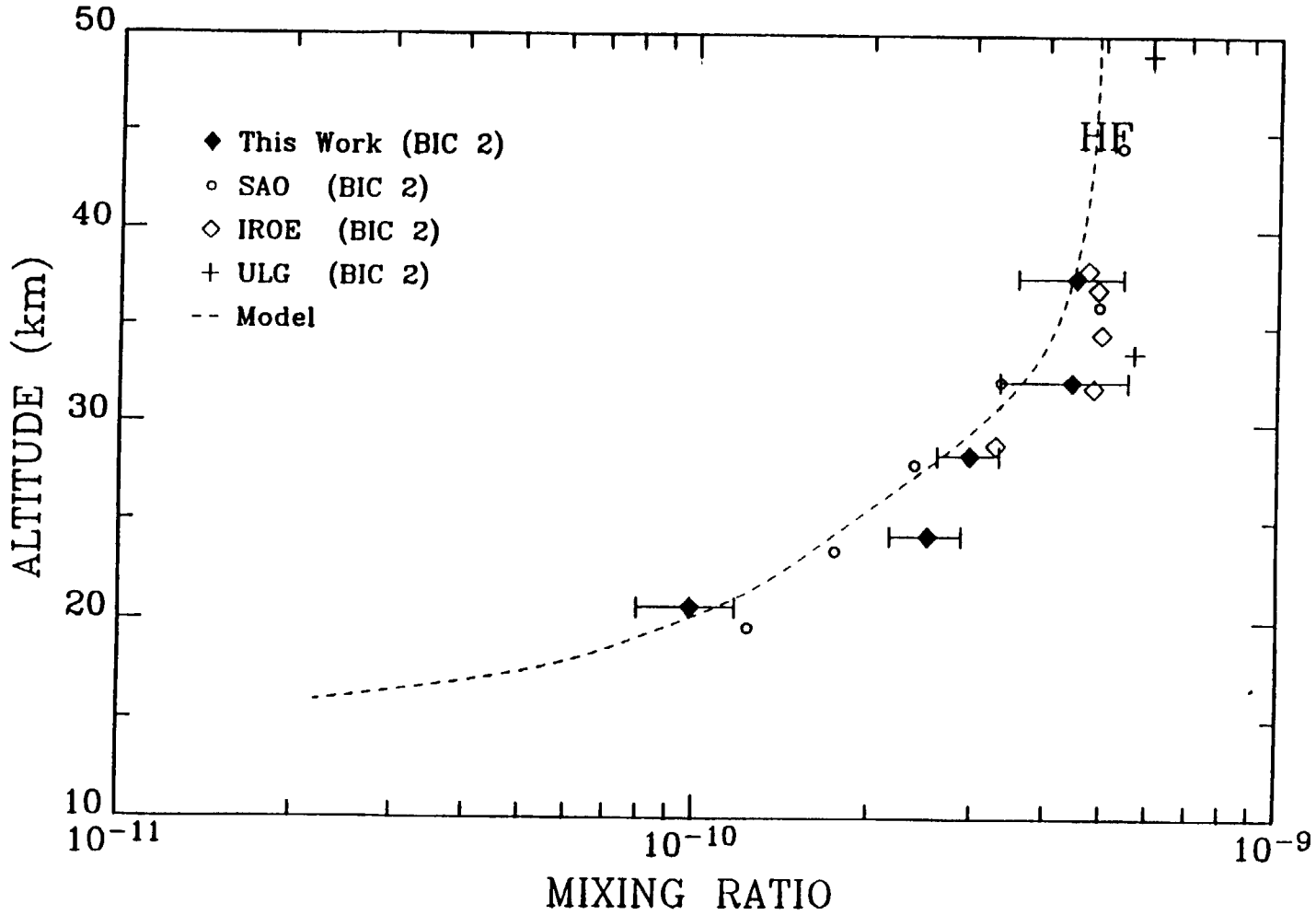
50
40
30
20
10
ALTITUDE (km)
This Work (BIC 2)
SAO (BIC 2)
IROE (BIC 2)
ULG (BIC 2)
Model
HF
10^{-11}
10^{-10}
10^{-9}
MIXING RATIO

Fig. 12

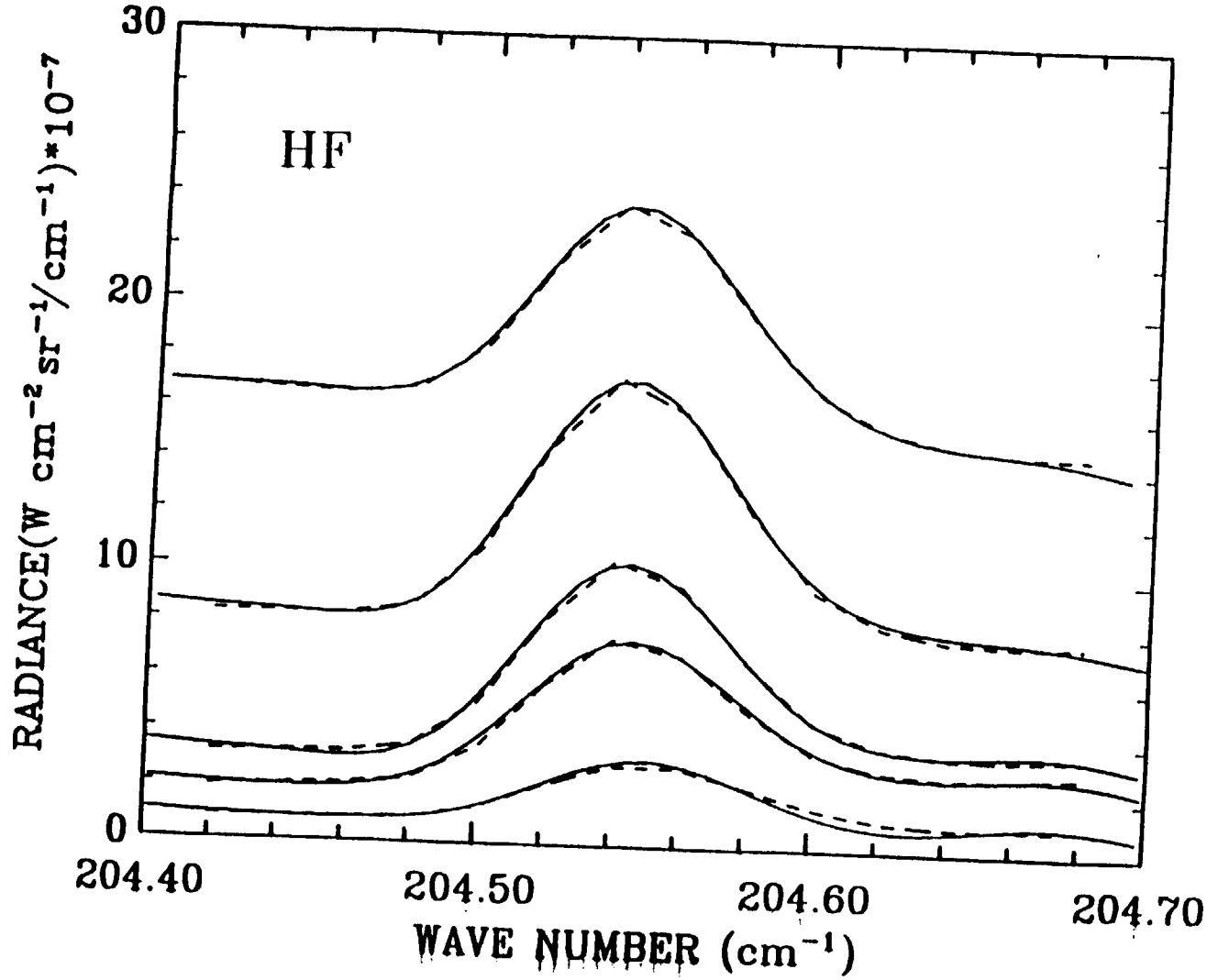
HF
30
20
10
0
RADIANCE(W cm^{-2} sr^{-1}/cm^{-1})*10^{-7}
204.40
204.50
204.60
204.70
WAVE NUMBER (cm^{-1})

Fig. 13

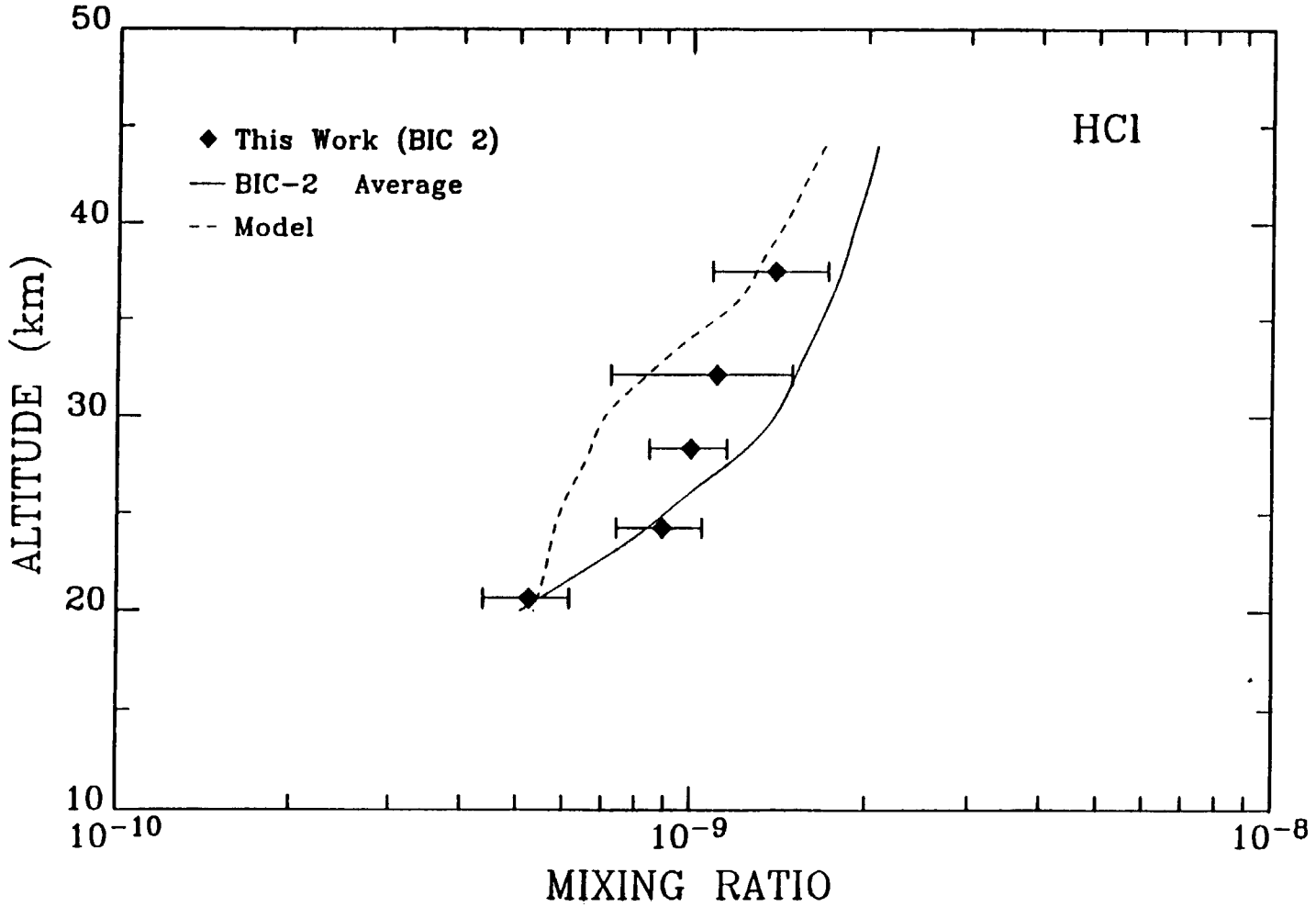
50
40
30
20
10
ALTITUDE (km)
◆ This Work (BIC 2)
— BIC-2 Average
-- Model
HCl
10^{-10}
10^{-9}
10^{-8}
MIXING RATIO

Fig. 14

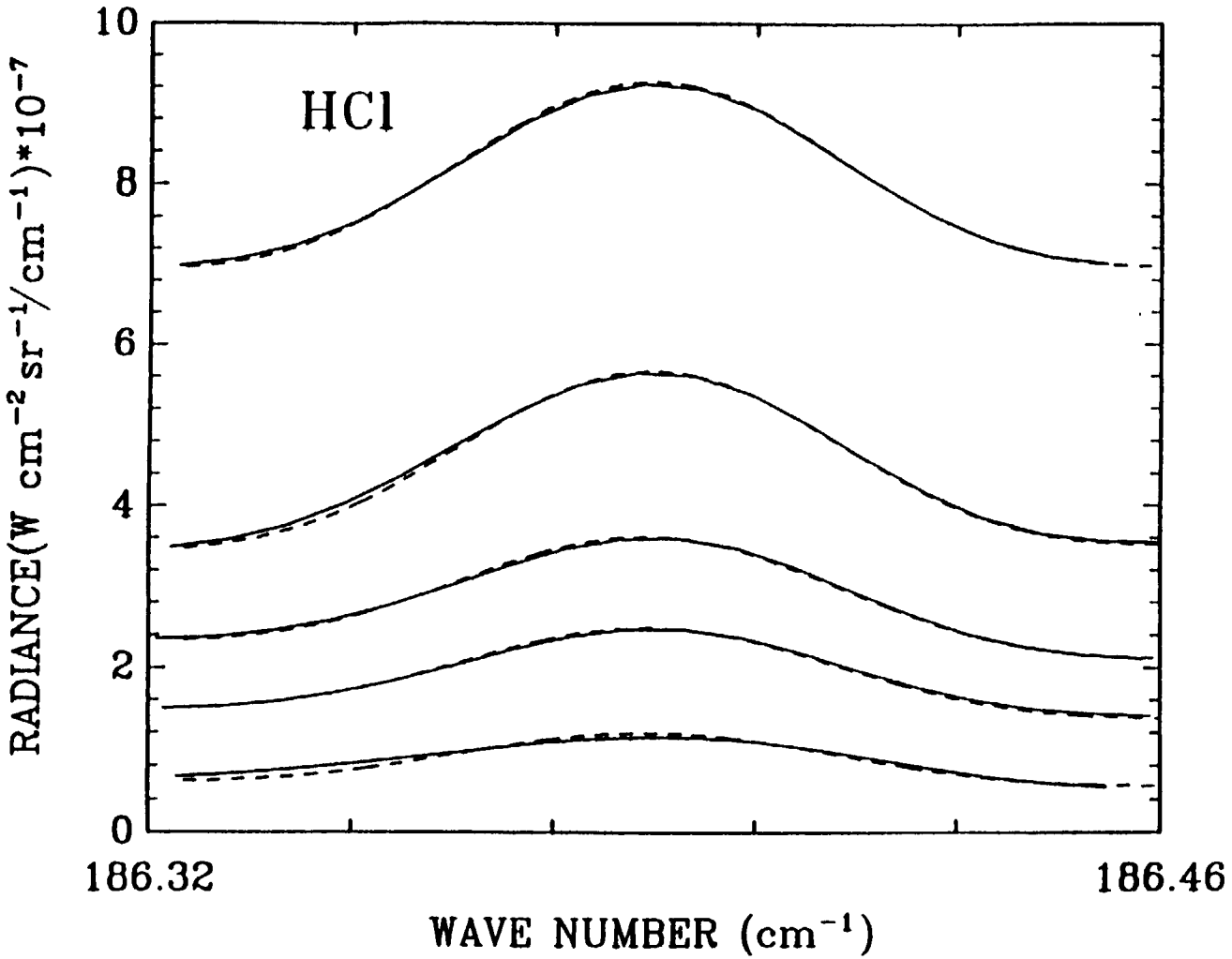
HCl
RADIANCE(W cm^{-2} sr^{-1}/cm^{-1})*10^{-7}
10
8
6
4
2
0
186.32
186.46
WAVE NUMBER (cm^{-1})

Fig. 15

...with no ClO (the lowest energy channel) observed in any experiments. ... a similar study on ClOOCl reported a quantum yield of ... for Cl atom products.

... have reinvestigated the photodissociation of chlorine nitrate ... Crossed Molecular Beams Apparatus. Under the collisionless ... conditions of this experiment, the primary photofragments are ... directly detected, and their translational energy and angular ... distributions measured.

... observed conclusively that the photolysis of chlorine nitrate ... to the significant production of ClO, approximately ... remaining 35% in one other channel, forming Cl atoms. ... sensitivity of the apparatus for ClO versus Cl has been ... experiments on the photodissociation of chlorine dioxide.

This experiment is the first direct detection of ClO fragments from ... photolysis and demonstrates that there is a substantial ... for breaking the weakest bond. Breaking the weakest bond ... a ClOOCl leads to ClO products as well. The failure of the chlorine ... experiments to detect the large ClO yield raises doubts about ... atom quantum yield measured in the related ClOOCl ... experiment. ClO products would result in a null catalytic ... and a significant yield of ClO would diminish the ozone loss ... by current models.

Coffee Break

1515h

Changes in Stratospheric Ozone due to the Eruption of Mt. Pinatubo

... and M Schoeberl, (Both at: NASA/ Goddard Space Flight Center, Code 916, Greenbelt, MD 20771)

The massive eruption of Mount Pinatubo on June 15-16, 1991 has renewed our interest in understanding the possible impact of volcanic eruptions on stratospheric ozone. This paper, which is based on the Nimbus-7 TOMS and NOAA-11 SBUV/2 measurements, studies the spatial and temporal characteristics of the aerosol clouds and the global changes in total ozone and ozone profiles after Pinatubo eruptions. It is shown that the Pinatubo eruption took place during the easterly phase of the QBO and as such presents a different dynamical scenario for the changes in stratospheric ozone as compared to El Chichon eruption which took place during the westerly phase of the QBO. A preliminary analysis of these data sets suggests that after the QBO effects are taken into account, the changes in column ozone attributed ... eruptions are no more than 2-4% - a conclusion in general ... with a similar study of the El Chichon effects on ... ozone.

A328-9 1530h

The Potential Role of Heterogeneous Processes on Volcanic Aerosols in Chemical Perturbations of the Stratosphere

C Granier, G. Brasseur (National Center for Atmospheric Research*, Boulder, CO 80307-3000 USA; 303--497-1456; Internet: brasseur@ncar.ucar.edu), and M. Mozurkewich (Chemistry Department, York University, Toronto, Canada; 416--736-5796)

Heterogeneous reactions on the surfaces of stratospheric particles ... have an important influence on the levels of ozone depletion ... from increased concentrations of anthropogenic chlorine ... compounds in the atmosphere. Parameterizations of the hetero- ... genous processes occurring on the surface of the stratospheric sulfate ... aerosols have been introduced in a two-dimensional chemical/ ... transport model. The magnitude of the changes of the strato- ... spheric minor species under these processes depends greatly upon the ... values adopted for the heterogeneous reaction probabilities. Sensitivity studies will be presented, based on our most recent ... laboratory measurements.

The analyses of measurements performed in the northern midlatitude ... region shows that the ozone abundance has significantly decreased in ... late 1982 and 1983, which could be related to the eruption of El Chichón, in Mexico. The June 1991 eruption of Mt. Pinatubo, in the Philippines, has injected at least twice as much sulfur in the ... atmosphere than El Chichón. Simulation results for these different ... aerosol loads will be discussed. Evaluations of the impact of volcanic ... eruptions on the future evolution of the atmosphere will be given.

*The National Center for Atmospheric Research is sponsored by the National ... Science Foundation.

A328-9 1545h

A Modeling Study of the Quasi-biennial Oscillation in Ozone

Peter Hess, (National Center for Atmospheric Research*, Boulder, CO 80307-3000; 303--497-1443; Internet: hess@acd.ucar.edu)
(Sponsor: Claire Granier, AGU Member)

A quasi-biennial oscillation (QBO) in total ozone has been well documented in the equatorial stratosphere, as well as in the extratropics. The equatorial ozone oscillation has been explained in terms of the dynamical quasi-biennial oscillation. However, the extratropical oscillation has not yet been satisfactorily explained.

In the modeling study discussed here we simulate stratospheric ozone transport using winds generated with a three-dimensional mechanistic stratospheric model. The mechanistic model is run with either easterly or westerly winds in the lower equatorial stratosphere, thus simulating the easterly and westerly phases of the dynamical QBO. Ozone chemistry is parameterized through the relaxation of the modeled ozone distribution to a climatological distribution. Both the climatological ozone distribution and the relaxation timescale (specified as a function of latitude and height) are specified from a two dimensional stratospheric model with fairly complete chemistry. In accord with observations the total ozone increases in the polar regions during the easterly phase of the dynamical QBO. The polar vortex is more disturbed during the easterly phase of the QBO than during the westerly phase. As well as examining the relation between the polar ozone concentrations and the dynamical QBO, we examine the effects of the parameterized ozone chemistry on the extratropical QBO and the relation between the equatorial and extratropical ozone QBOs.

*The National Center for Atmospheric Research is sponsored by the National Science Foundation.

A328-10 1600h

Ozone Vertical Column Abundance Measurements: Winter and Spring, 1992

C R Burnett (Department of Physics, Florida Atlantic University, Boca Raton, FL 33431-0991)
E B Burnett (NOAA Frits Peak Observatory, PO Box 39, Rollinsville, CO 80474)
R N Cooksey (Department of Physics, University of Wisconsin, 1150 University Ave, Madison, WI 53706)

The 15-year series of ON measurements at Frits Peak Observatory has been continued through Spring, 1992. This includes the period of initial intrusion of the Mt. Pinatubo aerosols over the observatory site in Colorado (40° N). Analyses of measurements up to the present time are presented. Additional analyses of the entire 1977-1992 ON data base as it relates to the photochemistry of the lower stratosphere are discussed.

Research supported by NSF ATM 88-16305, NASA NAGW-949, and the NOAA Aeronomy Laboratory.

A328-11 1615h

Stratospheric Minor Constituent Distributions from Far Infrared Limb Thermal Emission Observations

M M Abbas (Space Science Laboratory, NASA Marshall Space Flight Center, Huntsville, AL 35812; 205--544--7680)
W Traub and K Chance (Harvard Smithsonian Center for Astrophysics, Cambridge, MA 02138; 617--495--7408)

The mixing ratio profiles of O_3, $H_2{}^{16}O$, $H_2{}^{18}O$, $H_2{}^{17}O$, HF, and ECl_4 have been retrieved from far infrared limb thermal emission observations in the 80--220 cm^{-1} spectral region. These observations were made with a balloon-borne Fourier transform spectrometer with an unapodized spectral resolution of 0.033 cm^{-1}, carried out as a part of the Balloon Intercomparison Campaign (BIC-2) on June 20, 1992. The retrieved constituent profiles are compared with the measurements made with other instruments on the BIC-2 flights, with a focus on the stratospheric distribution of water vapor isotopes. The results for the concentrations of $H_2{}^{18}O$ and $H_2{}^{17}O$ obtained in this study indicate statistically normal distributions with no enhancement or depletion.

A328-12 1630h

Three-Dimensional Simulation of Stratospheric CO_2

Timothy M. Hall and Michael J. Prather (Both at: Goddard Institute for Space Studies, 2880 Broadway, New York, New York 10024; telephone: (212) 678 5592)

We have performed a ten year three-dimensional tracer simulation of CO_2 in the stratosphere. The model employed has a horizontal resolution of 8 by 10 degrees and 21 levels in the vertical from ground to approximately 0.015mb. The GISS general circulation model provides the advecting winds, and the bottom layers are forced with a seasonal cycle and secular trend derived from observations. The secular trend allows model prediction of the age of stratospheric air relative to tropospheric air. We also report on the predicted propagation of the seasonal cycle into the stratosphere. These predictions are briefly compared to observations.

A New Version of A Self-Validation Method and Its Application to The SBUV/2 NOAA-11 Backscattered Ultraviolet Data

X. Gu and C. Wellemeyer (Both at: Hughes STX Corporation, 4400 Forbes Blvd., Lanham, Md. 20706-8000)
R.D. McPeters (NASA/Goddard Space Flight Center, Code 916, Greenbelt, Md. 20771)

The SBUV/2 NOAA-11 non-local noon equator crossing time and its orbital drift makes the ozone determination more complicated. A new version of the "Pair Justification" method applied to the Nimbus-7 TOMS data has been developed particularly for the NOAA instrument to identify and remove the effects of the degradation of the solar diffuser on the derived total ozone. Preliminary results are obtained and compared with those from an onboard Hg Lamp calibration system. No significant statistical difference is found from the comparisons, indicating the success of both methods with environment calibrations and/or validations. Over the period of 2.5 years the A pair (3125-3312 nm) calibration error is about 0.5 DU according to the self-validation method, and 1 DU according to the Hg lamp system. The SBUV/2 NOAA-11 diffuser has proven to be quite stable with very little degradation as the total ozone wavelengths.

Computer simulations are performed to evaluate the sensitivity of pairs to the profile shape. For the purposes of the self-validation of the NOAA-11 data, the new D' pair (308.8-312.5 nm) is demonstrated to be superior to the D pair (308.8-312.5 nm), which has done excellent job for the SBUV ozone determination.

A

A41A CC: 405 Thurs 0830h
Radiative Forcing of Climate
Presiding: V Ramaswamy, NOAA/GFDL; R E Dickinson, Univ of Arizona

A41A-1 0830h

Variation of Radiative Forcing of Trace Gases With Latitude

K P Shine (Meteorology Department, Reading University, 2 Earley Gate, Reading RG6 2AB, UK; 44-734-318403)
(Sponsor: V Ramaswamy)

The radiative forcing of different trace gases varies with latitude because of shifts in the Planck function with temperature and changes in concentrations of water vapour and other constituents.

Narrow-band radiative transfer modelling results are presented which illustrate these effects. For example, the effect of chlorofluorocarbons relative to carbon dioxide falls off rapidly with latitude as the energy available at around 10 microns decreases. A similar effect is not seen for methane because the effects of overlap of absorption bands with water vapour also drops off with latitude.

These latitudinal variations are shown to only slightly alter the forcing calculated using a hemispheric-mean profile. The hemispheric average effective carbon dioxide is calculated and, because of the above mentioned effects, it is shown to vary with season.

A41A-2 0845h

Global Lower Stratospheric Ozone Depletions: Effect on Radiative Forcing of Climate

M.D. Schwarzkopf, V. Ramaswamy (Geophysical Fluid Dynamics Laboratory/NOAA, P.O. Box 308, Princeton, NJ 08542; Tele: 609-452-6521 Fax:609-987-3063)

The observed global reduction of ozone in the lower stratosphere during the 1980s has resulted in a negative greenhouse forcing of the surface-troposphere system. Calculations using the decadal ozone depletions obtained from TOMS measurements suggest that the globally and annually-averaged forcings are comparable to the positive forcings from the decadal CFC increases. In polar latitudes, the forcings become as great as those from decadal changes in all trace gases.

The radiative forcings have been obtained assuming no change in middle atmosphere dynamical heating. The forcings are sensitive to the shape and altitude of the ozone depletion profile.

ORIGINAL PAGE IS OF POOR QUALITY